Progressive Damage Analysis of Composite Laminates Under Compression

Sourabh Khedkar

A Thesis Submitted to
Indian Institute of Technology Hyderabad
In Partial Fulfillment of the Requirements for
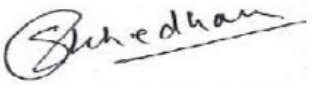The Degree of Master of Technology

भारतीय प्रौद्योगिकी संस्थान हैदराबाद
Indian Institute of Technology Hyderabad

Department of Mechanical Engineering

June 2014

Declaration

I declare that this written submission represents my ideas in my own words, and where ideas or words of others have been included, I have adequately cited and referenced the original sources. I also declare that I have adhered to all principles of academic honesty and integrity and have not misrepresented or fabricated or falsified any idea/data/fact/source in my submission. I understand that any violation of the above will be a cause for disciplinary action by the Institute and can also evoke penal action from the sources that have thus not been properly cited, or from whom proper permission has not been taken when needed.

(Signature)
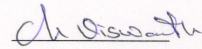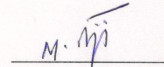
Sourabh Khedkar

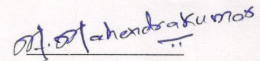(Sourabh Khedkar)

ME12M1025

(Roll No.)

Approval Sheet

This Thesis entitled Progressive Damage Analysis of Composite Laminates Under Compression by Sourabh Khedkar is approved for the degree of Master of Technology from IIT Hyderabad
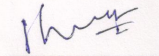
(Dr. Viswanath Chinthapenta, Asst. Professor, IIT Hyderabad) Examiner
Dept. of Mechanical & Aerospace Engineering
IITH

(Dr. M. Ramji, Asst. Professor, IIT Hyderabad) Adviser
Dept. of Mechanical & Aerospace Engineering
IITH

(Dr. Mahendrakumar Madhavan, Asst. Professor, IIT Hyderabad) Co-Adviser
Dept. of Civil Engineering
IITH

(Dr. S. Suriya Prakash, Asst. Professor, IIT Hyderabad) Chairman
Dept. of Civil Engineering
IITH

Acknowledgements

Dedicated to

My Grandfather
and
Grandmother

Abstract

The behavior and strength of carbon fiber reinforced polymer (CFRP) panels subjected to tensile loading has been studied extensively by various researchers over several decades. While its tensile behavior is well understood, but its compressive behavior is not. To better understand the compressive behavior, it is important to develop accurate compression test method. In addition, the behavior of the CFRP laminates having open cut out act as stress raisers under given loading conditions. The structures are susceptible to damage near these discontinuities leading to progressive failure. The progressive failure analysis (PFA) broadly involves damage initiation, damage evolution and stiffness degradation due to the damage. It becomes very complex in case of composites due to inhomogeneity, anisotropic nature and multiple failure modes.

In this study, Suppliers of Advanced Composite Materials Association (SACMA) and University of California Santa Barbara (UCSB) for open hole compression (OHC) test fixture is studied. Through testing, it is found that UCSB compression test method would be good alternate option for compression test as it is light weight, require smaller specimen and provide consistent and accurate results as compared to SACMA fixture. Further investigation of compressive behavior of carbon fiber reinforced polymer is carried out for single hole followed by specimen having two holes of various configurations with a specially developed anti-buckling fixture using digital image correlation (DIC) technique. In addition, the whole field surface displacement and strain surrounding the hole is obtained and then compared with FEA. A three dimensional (3-D) progressive damage modeling (PDM) is developed for interacting multiple hole and repaired panel configuration. PDM is very helpful tool to predicts the failure initiation load, ultimate strength and failure mechanisms of open cut out, multiple hole and repaired panel under compression load. It is found that matrix cracking and fiber-matrix shear failure followed by delamination plays a dominant role in final failure of CFRP panel under compression. Meanwhile in repaired panels, damage is influenced by localized patch debondings due to shear failure in adhesive layer. In addition, load-deflection behavior as well as the damage progression is predicted by PDM involving FEA and they are compared with experimental results. They are found to be in good coherence thereby confirming the accuracy of PDM implementation.

Contents

List of Figures

List of Tables

Chapter 1

Importance of Compression in Composite Material

1.1 Introduction

The invention of composite materials and its utilization in various industries such as aerospace, marine, transportation, sports equipment, etc. have opened up new methods for the design of high performance structural components and enabled engineers to create lighter and stronger structures with more complex shape than had previously been feasible with metal or wood.

Composite material [14] is usually defined as a combination of two or more distinct constituents or phases separated by a distinct interface. As a result, they offer desirable combination of properties based on principle of combined action to meet a particular requirement which may not be possible if any one of the constituent was used alone. One of the constituent is called as reinforcement and the one in which it is embedded is known as matrix. Composite materials are classified in accordance with the type of matrix material into metal matrix, ceramic matrix or polymer matrix composites. Composites are further classified based on arrangement and geometry of reinforcement into particulate reinforced (random, preferred orientation) and fiber reinforced (continuous, discontinuous, aligned, random) composites. The aerospace industry has benefited greatly from advances in composite material technology. Composite material technology is widely useful in vertical-takeoff -landing aircraft and helicopters, military fighter jets, sail planes and a wide variety of hand gliders and ultra-light aircraft.

Carbon fiber reinforced polymer (CFRP) is characterized by the superior mechanical properties such as low density, high strength, higher stiffness and high fatigue life whereas in chemical property it is corrosion resistance and physical properties such as high service load which made them ideal choice of material in diverse application. CFRP composites have seen a remarkable increase and extensive usage in today's commercial aircrafts. Efficiency

and performance can be improved by decreasing the aircraft weight through considerable usage of composite materials in the aircraft structures. Advanced fiber reinforced composite materials were originally developed for aerospace industry to use as primary structural materials. All the major aircraft manufacturers have been trying to develop the next generation of airliners using increased percentage of composite materials. Initially only a few components were replaced with composite material for eg. Airbus A300, while with the latest developments, the Boeing 757, 767, 777, 787 and Airbus A350 are employing significant amount composite materials. The Boeing 787 Dreamliner makes greater usage of composite materials than any previous commercial airliner. Up to 50% of the Boeing 787 Dreamliner aircraft is built using CFRP and other composite materials including the primary structures namely fuselage and wing. A350 XWB has roughly 53% of composites utilized in the fuselage and wing. Utility of composite materials in Boeing 787 Dreamliner aircraft is illustrated Fig. 1.1 [15]. With time and service, composite materials tend to degrade and damage, and understanding its damage phenomena is of primary concern. Increased use of CFRP in structural parts with high mechanical property needs better understanding about the mechanical behavior of CFRP structures.
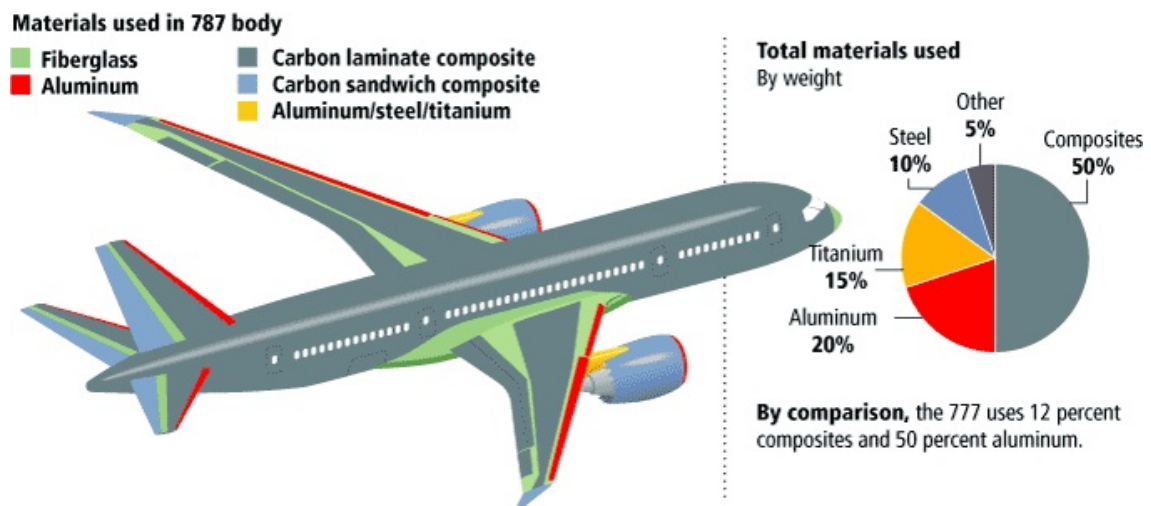
Figure 1.1: Breakdown of materials used in Boeing 787 Dreamliner [1]

1.1.1 Importance of Compression Test Methods

Most structures experience both tensile and compressive forces and their failure behavior changes accordingly. For example, wings in aircraft and hull in ship structure typically experience compression under service load. CFRP laminates possess superior tensile properties, but their compressive strengths are often less satisfactory. Budiansky and Fleck, [16] have concluded that compressive strengths of unidirectional carbon fiber-epoxy laminates in many instances are less than 60% of their tensile strengths. Compression test is diffi-

cult because the data are usually considered to be less accurate and difficult to reproduce. In compression test, little loading in off axis or misalignment, leads to premature buckling. Ideal compression test is one in which the compression specimen is loaded in pure axial compression. Thus, to understand compressive failure, an accurate compression test method is required. However, till date many fixture were developed for compression test method such as IITRI fixture, ASTM D 695 fixture, Celanese fixture, Northrop fixture, SACMA fixture, etc. All fixture have advantages and disadvantages. Therefore, it is important to use the fixture for studying the compressive behavior of CFRP laminates.

1.1.2 Multiple Holes in Composite Structures

Most of the structures need the presence of multiple holes and cut-outs in them mainly for joining of different structural parts, damage inspection and for installation of electrical and hydraulic piping system etc. [17]. Such holes are source of stress raisers due to geometrical discontinuity and act as damage initiation site. Stresses around the hole are three dimensional by nature due to the presence of interlaminar stresses at free edges. In repairs, multiple holes in different patterns or arrays result when fastened the patch laminate to parent laminates with moderate thicknesses are mechanically. The presence of multiple interacting holes makes the problem still more complex. The failure mechanism and strength prediction of such structures is of great interest mainly because of practical applications. Fig. 1.2 shows the wing covers of Airbus A350 XWB made from CFRP with multiple cut-outs.

1.1.3 Patch Repair in Composite Material

Compared to conventional metallic structures, the composite structures are prone to damage like matrix cracking, fiber breakage, debonding and delamination due to accidental impact, bird strike, fatigue loading and environmental degradation, during its service life. The initiation of damage in a composite laminate occur when each ply or a part of it in the laminate fails in any of these failure modes over a certain region of the structure. These damages will result in reduction of their residual load bearing capability. Thus structural strength of composite laminates from initiation of damage to final failure is quite significant. Beyond the final failure point, the structure cannot carry any load and could lead to catastrophic failure. Depending on the extent of damage and the constraints of operational condition, the following actions are taken: temporary repair, permanent repair or replacement to regain its structural integrity. But due to high cost of the composite structures/retrofitting, it is not feasible to replace the damaged structure and hence the best possible action is to repair. These repairs can possibly be achieved either by using mechanical fasteners or adhesively bonded patches. The adhesive bonded patch repair is preferred over the mechanical fastener due to stress risers acting at the fastener holes resulting in higher stress concentration factor (SCF). Hence, it is prone to more damage compared to the bonded

Figure 1.2: Wing covers of Airbus A350 XWB made of CFRP [1]

patch repair. In contrast, the adhesively bonded repair offers smooth load-transfer from the panel to patch as large load transfer areas are available, making it much stiffer than mechanical joint. Adhesively bonded repairs are also highly cost-effective and are a proven method for enhancing the structural integrity by reducing the stress concentration in the damaged area. They also provide very high level of bond durability under various operating conditions [18] as fiber reinforced composites are bonded in nature.

The scarf and externally bonded patch repair [19] methodology are mostly preferred in the adhesively bonded repair. The scarf repair is mainly adopted where surface smoothness is essential and applies to the repair of critical load-bearing structures where load concentration and eccentricities must be avoided. While, the externally bonded patch work is preferred for repair of less critical load bearing structures. The manufacturing of a scarf repair requires a higher level of expertise than the external patch and it results in removal of excessive amount of the undamaged material towards achievement of a given scarf angle. Also, the bonding of external patches is relatively simpler than the scarf approach and can be accomplished faster. In external patch repair technique, the damaged material is removed by cutting a hole, the parent panel is then cleaned and applied with filler and patches to the adhesive material. External patch repair is considered as a temporary repair and aims to restore the structural strength which permit aircraft operational until a perma-

nent repair can be carried out. From the geometrical point of view, the repair can possibly be achieved by bonding the patch over one side (un-symmetrical repair) or on both sides (symmetrical repair) of the panel. However, behavior of single sided patch repair is quite complex as there is an additional bending effect due to the shift in the neutral axis of the repaired panel. But single or double sided external patch repair selection is done on the availability of space and constraints. Fig. 1.3 shows the application of bonded patch repair on an aircraft.
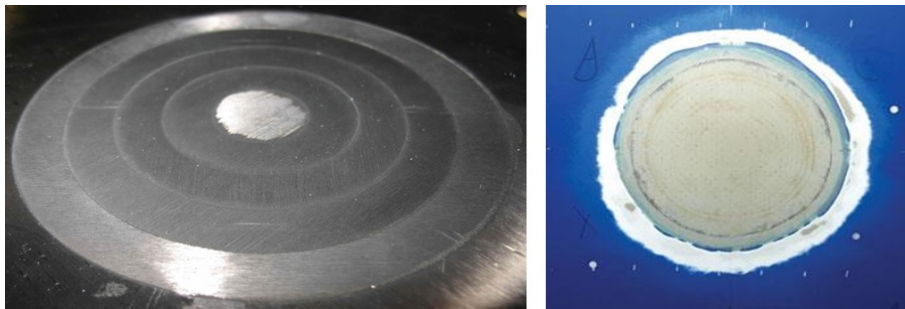
Figure 1.3: Application of bonded patch repair on an aircraft [2]

1.2 Literature Reviews

1.2.1 Compression Study

The compressive behavior of CFRP is complicated due to the fact that the fibers undergo local micro-buckling which is not observed in tension. Rosen [20] presents one of the earliest works on compressive response of composites, where local micro-buckling is considered as the governing mechanism in compressive failure. In micro-buckling, fibers are considered as individual columns surrounded by matrix material that act independently. In addition to micro-buckling, the same authors had proposed another model known as compressive kinking which is a form of micro-buckling. In kinking, the deformation is localized in a band in which the fibers are rotated to a large extent whereas during micro-buckling, the fibers act individually and no bands are formed.

Many researchers have studied the failure in fiber reinforced laminated composite structures containing discontinuities, such as holes or notches which also includes progressive failure analysis of panel with single hole. Guynn et al. [21, 22] compared the damage zone at the edges of the hole to a crack with a plastic zone using Dugdale model [23] to predict the size of the buckled region as a function of compressive load for both carbon-epoxy and carbon-PEEK composite laminates. They concluded that a constant stress state in the damage zone does not accurately predict the compressive failure stress of the notched laminate and indicates a greater amount of stable micro-buckling growth than it is observed in prac-

tice. Soutis et. al. [24, 25, 26] has investigated the compressive fracture properties of carbon fiber/epoxy laminates. They reported that the failure mechanisms in all laminates were due to the micro-buckling in the [0°] plies, delamination between off-axis and [0°] plies, followed by plastic deformation. They also observed that failure was sudden and catastrophic and it occurred within the gauge section. Bazant et. al. [27] presented a size effect study of hole on compressive strength of fiber composites failing by kink band propagation. There are several standards for compression test widely followed in composite domain. Abdallah, M.G. [28] divided compression test fixtures into four groups based upon loading methods which are shear loaded, end-loaded, end-loaded and sidesupported, and others such as sandwich beam, rings and tubes. The research results indicate recommended the IITRI fixture and sandwich beam in four-point flexure as the best methods. Gedney et. al. [29] studied the comparison of ASTM standard compression test methods of Graphite/Epoxy composite specimens mainly through three test methods, namely, ASTM D 695, Modified ASTM D 695 (Tabbed and Untabbed) were examined. It was found that the Modified ASTM D695 with tabbed specimen yielded the most accurate results with the least amount of effort. Adams et. al. [30] studied the influence of specimen gage lengths and loading method on the axial compressive strength of a unidirectional composite material with the help of standard IITRI and modified ASTM D695. Berg et. al [31] studied unidirectional and quasi-isotropic laminates of glass/epoxy and carbon/epoxy were tested using the standard IITRI, Wyoming modified celanese, Wyoming end-loaded side-supported. Pearson et. al. [32] studied capabilities of compression test methods for evaluating unidirectional carbon fiber reinforced composites using ASTM D 3410 (Modified Celanese) and ASTM D 695 fixture. Carl and Anothony [33] studied different compression test standard which includes ASTM, RAE (Royal Aircraft Establishment) and SACMA (Suppliers of Advanced Composite Materials Association) and presented a comparative chart. Bardis et.al. [7] has introduced alternate compression test method for notched and unnotched composites named as UCSB fixture. Hodge et. al [34] studied the Northrop OHC test fixture and Boeing CAI fixture and presented the comparative chart.

1.2.2 Multiple Hole Compressive Study

Due to complex failure mechanisms in composite material, prediction of failure is difficult and plays an important role in research field of composites. Several researchers have attempted to model the compressive failure; here only a brief overview of literature is presented. Soutis et. al. [35, 36] used linear softening cohesive zone crack analytical model considering micro-buckling and delamination to predict the compressive strength of composite laminates. The results indicated that the single hole was found to be in good agreement between experimental and analytical results. But predicting cohesive zone properly is non trivial and requires accurate experimentation. Chang et. al. [37] have presented a progressive damage model (PDM) for notched laminated composites subjected to tensile loading.

Their model can assess damage in laminates with different ply orientations and predicts ultimate strength of notched laminates. Damage modeling is done with the help of material property degradation method (MPDM). Tay et. al. [38] have done progressive damage analysis (PDA) of composite laminate involving element failure method. They have used various failure theories and have applied it to different problems. Wang et. al. [39] and Ridha et. al [40] presented the progressive damage analysis of composite laminates containing a open-hole subjected to compressive loading using Hashin failure criteria and concluded that majority of the damage comprises of fiber-matrix shearing, matrix cracking and delamination. Recently, Ubaid et al. [11] have conducted both experimental and numerical study to predict the strength of CFRP laminates in presence of multiple interacting holes under tensile loading involving PDM in conjunction with finite element analysis (FEA).

1.2.3 Patch Repair Compressive Study

Soutis et. al. [41, 42] have studied the external patch-repaired CFRP laminates loaded under compression in which a numerical approach is used to predict the strength with the help of the cohesive zone modelling. Considerable amount of work has been performed in progressive damage analysis on repaired composite laminates. Liu and Wang [43] conducted experimental and numerical study to analyze the progressive failure analysis of open-hole composite plates bonded with external composite patches subjected to tensile load for the double-sided repaired panel. The results indicate that, the parameters of the patch not only influence the patch performance but also the failure mechanism of the repaired structures. Tay et al. [44] had studied the performance of the notched and double-sided repaired composite panel using progressive failure analysis. They have used the cohesive element to model the adhesive layers between the patch and panel. EFM and material property degradation method (MPDM) in conjunction with multi continuum theory (MCT) which is based on micromechanics are implemented in their analysis. Ridha et al. [45] had presented the traction-separation laws for progressive failure of bonded scarf repair of the composite panel. Cheng et al. [46] conducted the experimental and numerical study to investigate the tensile behavior of composite structures repaired by adhesively bonded external patches. They have also studied the damage evolution in repaired specimens under tensile fatigue loading using infra-red (IR) thermography. Bhise et. al. [47] had studied the optimization of circular composite patch reinforcement on damaged carbon fiber reinforced polymer laminate involving both mechanics-based and genetic algorithm in conjunction with three dimensional finite element analysis. Kashfuddoja et. al. [48] conducted experimental and numerical investigation of progressive damage analysis in external bonded patch repaired for the single and double-sided respectively of the CFRP laminates.

1.3   Motivation, Scope and Objectives

During the past fifty years, many studies have been focused to improve the understanding of compressive failure of composite materials. It is well known that the compressive failure of composite material is mainly caused by a combination of localized buckling of fibres, kinking and delamination [49]. Thus, to understand the in-plane compressive failure of the composite material, it is necessary to know about the compression test methods. Ideal compression test method is one in which the compression specimen is loaded in pure axial compression. So, misalignment or off axis loading will leads to bending in addition to axial load and may leads to the premature failure. To minimize non-axial forces, it is important to reduce errors associated with on specimen preparation techniques, specimen geometries and compression test fixture. American standard of testing material (ASTM), RAE (Royal Aircraft Establishment) and SACMA (Suppliers of Advanced Composite Materials Association) have come forward with different type of compression testing fixture. This thesis discusses about the SACMA (ASTM D6484) and UCSB open hole compression (OHC) test fixture. UCSB fixture is an good alternate option to all available fixture since it is light-weight, utilize the standardized hydrallic gripping arrangement and gives slightly more accurate and precise result.

Composite structures containing discontinuities, such as holes or notches due to mechanical fastener joining and installation of electrical and hydraulic piping system. Thus open hole compression (OHC) failure analysis ia a key area to be studied. Most of the reported work till date is on progressive damage modeling and stress analysis of an open cutout panel under tensile loading. Only few experimental and numerical works exist on progressive failure analysis applied to compressive failure of open cutout CFRP panel. The main focus of study is on the compressive failure of interacting open hole panel. No significant work has been reported in the literature related to PDA of multiple hole CFRP panel under compressive loading. This study is important since, wing of an aircraft or hull of a marine ship has multiple cut out for assembly purpose and their behavior under compression load is of primary interest. In addition, the governing design criteria for a structure are typically based on the lowest strength which in this case is the compressive strength of the CFRP laminate. Thus, there is a need to understand the failure mechanism and also to predict the strength of composite panel with multiple interacting holes subjected to compressive load. Here, a finite element based three dimensional PDM is developed for single and multiple open cutout panels which includes Configuration 1H (a single hole at center), 2HL (two holes in the longitudinal direction), 2HT (two holes in the transverse direction) and configuration 2HD (two holes placed in diagonal pattern at 45). Hashin's failure criteria is employed. The study is conducted on quasi-isotropic panel made of carbon/epoxy composite laminate of configuration $[+45/0/-45/90]_{2S}$ where zero degree orientation corresponds to the loading direction. Initiation and propagation of damage as well as failure mechanism has been investigated. Both failure initiation and ultimate failure load with and

8

without open-hole is predicted. The accuracy of developed model is assessed by comparing the numerical prediction with experimental results obtained using digital image correlation (DIC) technique. Also at critical location, strain values are obtained from DIC and the corresponding stress vs. strain plot is obtained for better understanding. In addition, the effect of spacing between holes on stress concentration factor (SCF) is investigated using FEA to optimize the distance for getting lower SCF value.

An extension of the research on open cut-outs is the repairs of composite panels by adhesive bonded external patch. Adhesive bonded repair is always preferred as it provides very high level of bond durability under various operating conditions [18] as fiber reinforced composites are bonded in nature. Since the demand of the composite application is increasing significant space and the composite material is prone to degrade with time and service. Therefore, it is necessary to understand the failure mechanism of bonded patch repaired composite laminates. Most of the reported work is on progressive damage modelling and stress analysis of bonded repaired panels of composite laminates under tensile loading. Here, focus is mainly on compressive failure behaviour study of bonded repaired panel. No significant work has been reported in the literature related to PDA of repaired CFRP panel under the compressive loading. Here, a finite element based three dimensional PDM is developed for opencutout, single and double side repaired panels under compression and is compared with experimental results. Hashin's failure criterion is employed to carry out the progressive failure analysis. The study is conducted on the quasi-isotropic panel made up of carbon/epoxy composite laminate of configuration $[+45/0/-45/90]_{2S}$ where zero degree orientation corresponds to the loading direction. Initiation and propagation of damage as well as failure mechanism has been investigated. Both the failure initiation and ultimate failure load before and after the repair is predicted. Failure of the adhesive layer leading to patch debonding is also studied. The accuracy of the developed model is assessed by comparing the numerical prediction with experimental results.

1.4 Thesis layout

Chapter 1 explains briefly about composite materials and importance of compressive test for composite material. A brief introduction of compression for multiple hole and repaired composite laminate is presented through literature review.

Chapter 2 explains various compression tests to study the compressive behavior of composite under compression. An introduction of SACMA and UCSB test method for compression is provided along with a comparison of experimental result of both fixtures with finite element analysis.

Chapter 3 deals with the development of a progressive damage model that can be applied to composite panels with multiple interacting open cut outs under compression load. A finite element model is developed dealing with the implementation of various aspects as

part of progressive damage model. It also explains about specimen preparation and DIC experimental procedure. Finally validation of numerical results is carried out using the DIC results.

Chapter 4 deals with the development of progressive damage model for single and double sided external patch repair in composite laminate under compression load. It explains about development of finite element model for implementation of progressive damage model.

Chapter 5 is on conclusion and recommendation for the future work.

Chapter 2

Compression Test Methods

2.1 Introduction

Many of the mechanical properties of CFRP and their constituents that are important in design are derived from tensile, shear and compression testing. It is necessary to perform the test properly to validate the results in such a way that CFRP will be subjected to in use. All three tests have the common feature that an external load is applied to a test specimen and the response of specimen measured with respect to the load. Out of all tests, compression test is difficult because the data are usually considered to be less accurate and difficult to reproduce. A possible explanation for this follows.

Tensile and shear test are relatively forgiving of fiber reinforcement misalignment, because the applied load is not likely to cause unexpected distortion or premature failure of the fiber reinforcement. But in compression test, the unidirectional fibers that are part of reinforcement are typically subject to bending in addition to axial load if the specimen is loaded off axis or misaligned while loading. Thus, the ideal compression test is one in which the compression specimen is loaded in pure axial compression. The development of specimen preparation techniques, specimen geometries and compression test fixture have thus proceeded with the goal of minimizing non-axial forces on the compression specimens.

2.2 Earliest test methods for Compression test

Compression test method for cylindrical rod specimen was compressed between spherical fittings in a test fixture which was developed by Texaco Experiment, INC. (TEI) [3] which is shown in Fig. 2.1(a). Limitation of this fixture is the difficulty in test specimen fabrication and only used for testing longitudinal compressive properties. Later Narmco Test method 303 as shown in fig 2.1(b) was developed as an improvement of TEI method. Here, specimen in panel form was clamped to a test fixture and then loaded in compression. Fig. 2.1(c) shows the modified fixture of Narmco fixture in which a flat specimen was supported on both sides with sandwich core material known as Sandwich Stabilized Fixture. The above

two methods had the limitation that damage occurred at ends of the specimen despite the constraints, and complex non-axial stresses resulted. The limitation of above two methods is overcome by the fixture outlined in ASTM D695 and Federal Test Standard 406 Method 1021 which are shown in Fig 2.1(d) and 2.1(e), respectively. In both the fixtures, there were end constraints and jigs used to support the test section. Both these methods introduced friction forces that resulted in misleadingly high moduli. To improve this limitation, the next development came in a form of the Celenese fixture, which is shown in fig 2.1(f). This method used split conical collet grips that slides into matching sleeves, which in turn fit into a snugly fitting cylindrical shell. This fixture introduced axial forces on the specimen by loading the sides of the specimen near the ends in shear. Thus, most of the damage to the ends of the specimens was eliminated, and a pure state of axial compression was achieved. This fixture has a limitation creating frictional stresses on specimen which would result in erroneous measurements of specimen stiffness. Further modification of fixture is discussed later, to overcome this problem.
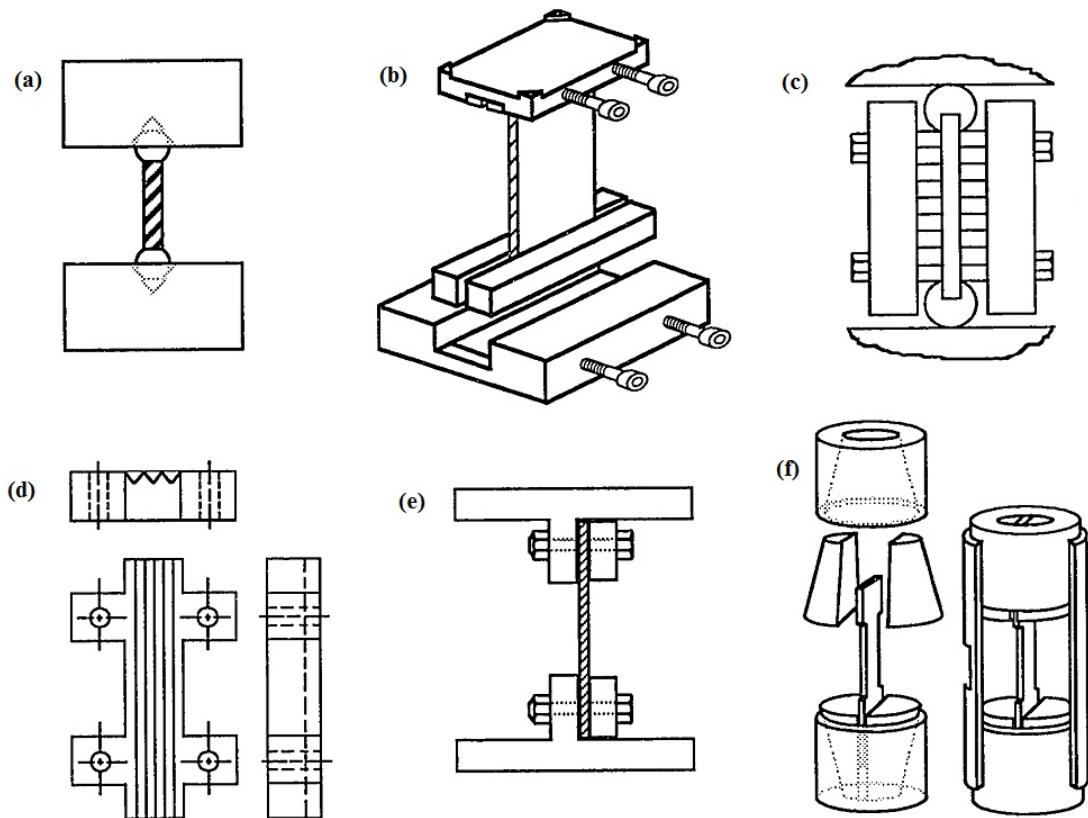
Figure 2.1: Various Compression Test Fixtures [11] (a) TEI fixture; (b) Narmco Test Method 303; (c) Sandwich Stanilized fixture; (d) ASTM D695-69 fixture; (e) Federal Test Method 406 fixture; (f) Celanese fixture [3]

2.3 Present Methods of Composite Compression Testing

The most commonly used present day methods of compression testing of composites have been classified by Camponeschi et. al. [50] into two major types. Type I testing consists of those methods where a specimen that is laterally unsupported and a relatively short gage length is compressed either by direct loading on its ends or by shear loading of its sides near its ends. Type II testing involves a relatively long gage length specimen fully supported along its sides and compressed in a manner similar to Type I specimens. Illustrations of specimens being tested by these two methods are shown in Fig. 2.2
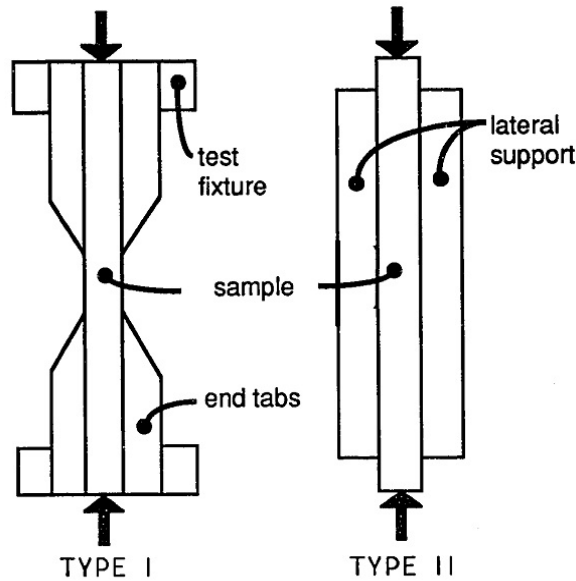
Figure 2.2: Illustrations of Type I & II Compressive Testing

2.3.1 Type I Testing Methods

One of the most widely used methods in compression testing involves the use of the Illinois Institute of Technology Research Institute (IITRI) fixture (ASTM D 3410) [51], which is shown in Fig. 2.3. The principle of operation for the IITRI fixture is derived from that of the celanese fixture, in that the compressive load is applied to the unsupported gage length by shear forces exerted by the fixture wedges through the specimens end tabs. In this fixture as the outer surfaces of the wedges are rectangular in shape and if oversized specimen pushes the wedges apart then it will still be in intimate contact with the load alignment block. Only disadvantage of the IITRI fixture is associated with its mass, in that it is difficult to work with.

Another commonly used test method consists of using a modified celanese fixture as shown in Fig. 2.4. It is similar to the unmodified Celanese fixture, except that there is a
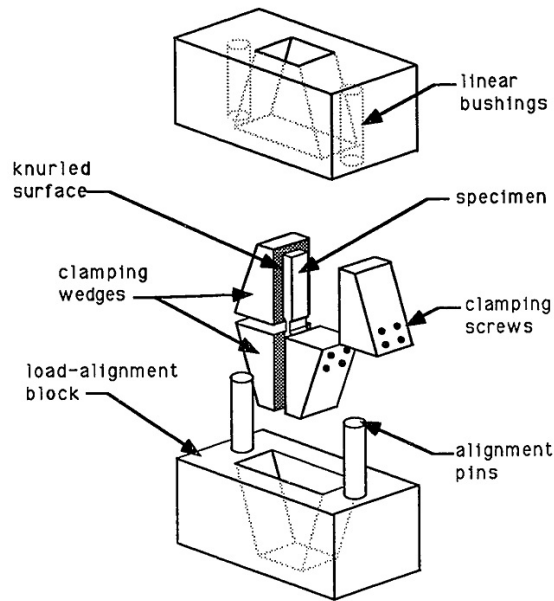
Figure 2.3: Exploded view of the IITRI test fixture (ASTM D 3410) [4]
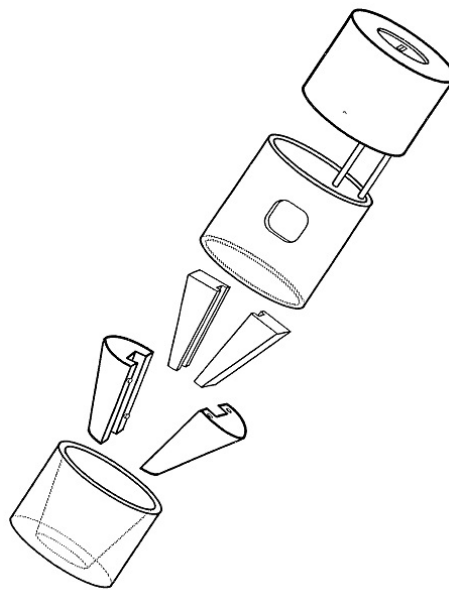
Figure 2.4: Exploded view of the Modified Celasese Test Fixture [5]

secondary set of rectangular grips within the cylindrical collet grips which eliminates the previously mentioned problem of non-intimate contact between the tapered surfaces [5].

Somewhat less commonly used test fixture is the Northrop fixture [6] as shown in Fig. 2.5. This fixture utilizes off-set unsupported specimen lengths and stability is maintained by the thick side supports. It can be seen that, this fixture is not truly a type I fixture, but

14

the rather a hybrid of type I and II fixtures, the thick side supports actually do lend some support to the gage section of the specimen. Advantages are being simple and relatively easy to use while disadvantages are that side supports induces friction in test specimen which will cause error in elastic modulus measurements.
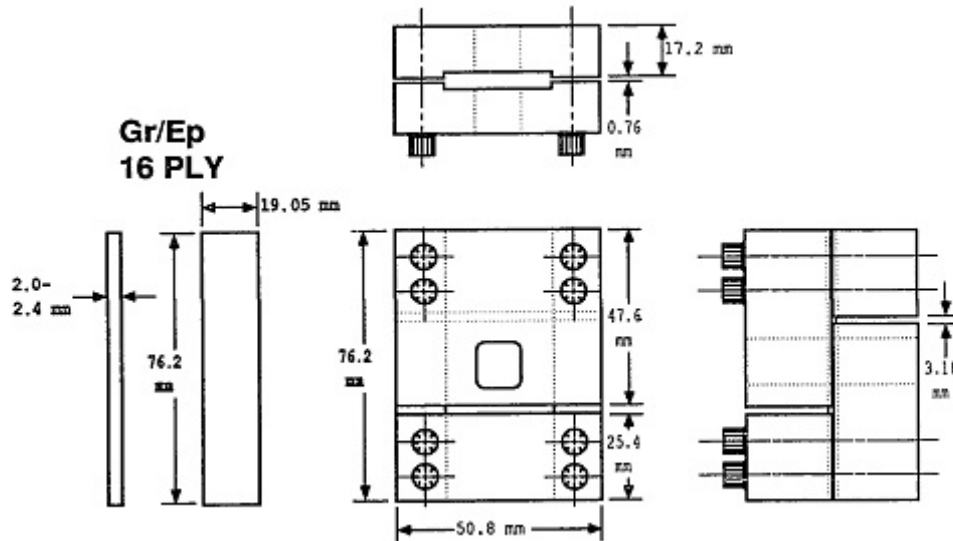
Figure 2.5: Northrop Fixture [6]

Another fixture that is hybrid of type I and II test methods is UCSB test fixture [7] which was recently developed as shown in Fig. 2.6. The silent feature of this fixture is that the test specimen can be subjected to combined end and side loading. It provides support extensions on the ends of the fixture which acts as self-contained. These ledges prevent the sample from slipping out of the fixture and provide a flat hardened bearing support surface. The fixture is lighter and smaller which allows the use of standard hydraulic grip testing facilities.
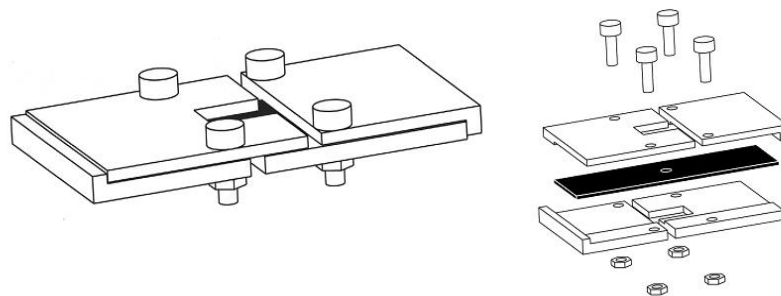
Figure 2.6: UCSB Test Fixture [7]

15

2.3.2 Type II Testing Methods

The first Type II testing method involves the use of the Southwest Research Institute (SWRI) [8] specimen setup as shown in Fig. 2.7. The fixture is designed such that the specimen is supported on both sides. The compressive load can be transferred to the specimen either by shear, in which the sides of the specimen that would be extending out from the specimen supports are gripped, or by direct compression of the ends of the specimen. The second test method consists of the use of the modified ASTM D695 [9] specimen supports as shown in Fig. 2.8. This support mechanism is similar to that of the SWRI support except that only the gage length of the specimen is supported.
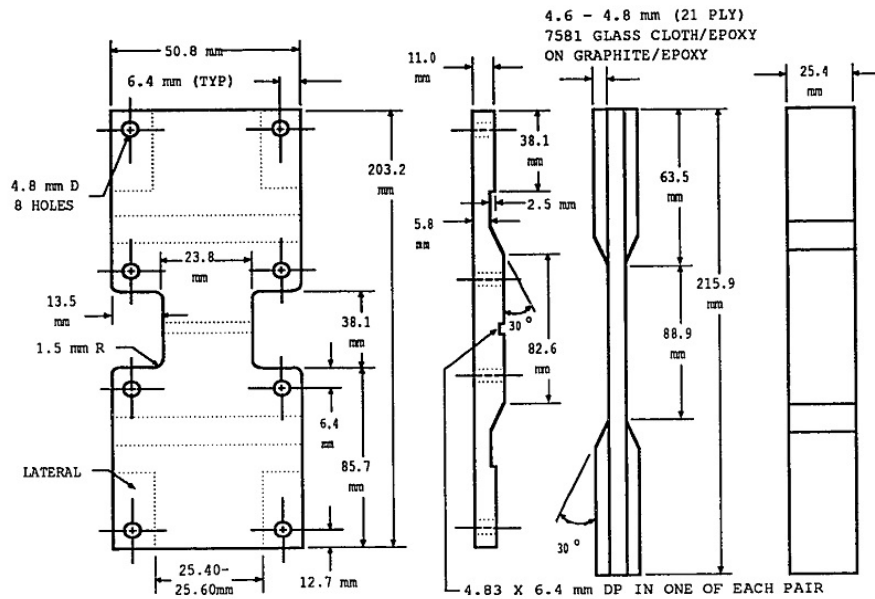
Figure 2.7: SWRI test Set-up [8]

The Suppliers of Advanced Composite Materials Association (SACMA) [10] in 1999 developed another end-loaded compression test; SRM 1R-94 (ASTM D 6484) is defined in MIL-HDBK-17 as shown in Fig. 2.9 and is used widely in USA and Japan. It provides two ways of performing compressive strength tests, generally on quasi-isotropic composite material, as well as multidirectional polymer matrix composite laminates reinforced with high modulus fibers, Hydraulic Grip Loading and End Loading. In Hydraulic Grip Loading, the specimen/fixture assembly is clamped in hydraulic wedge grips. The force is transmitted by shear into the support fixture and then is transmitted by shear to the test specimen. While in end loading, the specimen/fixture assembly is placed between flat compression platens, such that the specimen and fixture are end-loaded. The portion of the force initially transferred into the support fixture is transmitted by shear into the test specimen. The untapped specimen is gripped securely by two sets of long grip and short grip are bolted
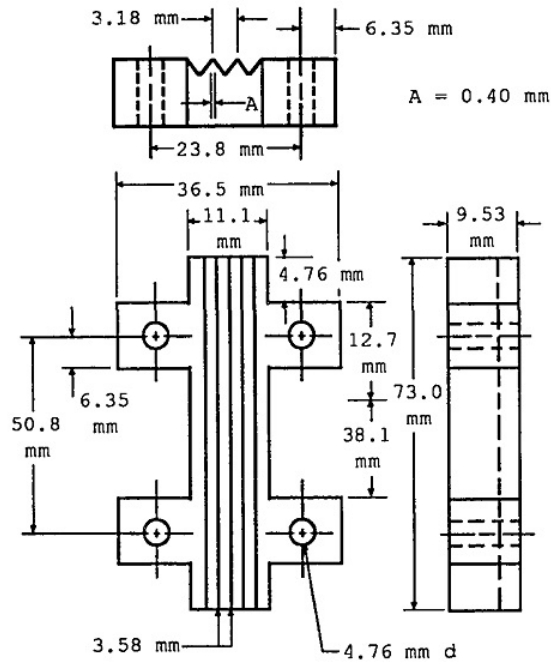
Figure 2.8: Modified ASTM D695 test setup [9]

to the fixture to constrain the main pieces, guiding the specimen into pure compression. A small window opening near the center of the fixture are present to give clear view of the failure of Open Hole Compression (OHC) or to allow for the placement of strain gauge. The disadvantage of this fixture that it is little bulky in overall size so making it difficult to handle, relatively large specimen size and require clamping pressure in the test grips.

2.4   Comparison of SACMA and UCSB Test Method

In this chapter, comparison is made between the compression test standard provided by SACMA 1R-94 and UCSB fixture. The overall UCSB fixture weighs only 0.72 kg which around 4.25 kg lower than the SACMA fixture. The smaller mass facilitates ease of handling, specimen loading, and testing compared to heavier fixtures like SACMA and ASTM D3410. The overall thickness, in the through-the-thickness direction (normal to the plane of the sample), is only 10.2 mm when fully assembled with a 3 mm thick specimen, as opposed to 33 mm for the SACMA setup. This allows the use of standard hydraulic grips without the necessity of purchasing larger, more expensive grips. Experimental results obtained from SACMA 1R-94 and UCSB fixture are validates the finite element analysis (FEA).
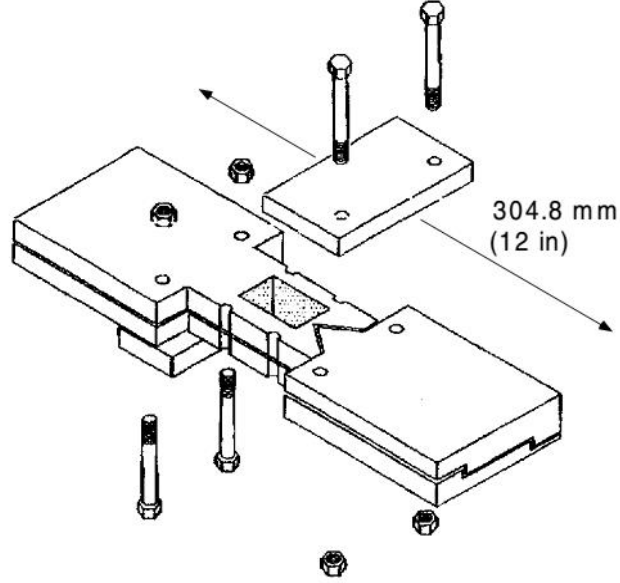
Figure 2.9: SACMA Test Fixture (ASTM D 6484) [10]

2.4.1 SACMA and UCSB Test Specimen Size

The SACMA fixture was designed around 305 x 36 x 3 mm test coupon with a 5 mm diameter hole at its center while the UCSB fixture was designed around 130 x 36 x 3 mm test coupon with a 5 mm diameter hole at its center as shown in Fig. 2.10 (a) and (b) respectively. Despite the smaller sample size for the UCSB fixture, the applied test load is still sufficiently far from the specimen hole to obtain accurate test results, as confirmed by a series of ANSYS 13 finite element analyses, discussed below.

Figure. 2.11 shows the meshed and loaded 3-D finite element analysis (FEA) models for the SACMA sized and UCSB-sized quasi-isotropic OHC samples used in the comparison analysis. The specimen is modelled using SOLID 186 element, which is a 20 noded brick element. The entire model contains a mapped mesh configuration. The mesh pattern surrounding the hole is kept very fine to capture the high stress gradient around it. The mesh around the circular hole has a total of 9216 elements (96 circumferential; 12 radial; 8 elements through the thickness). Away from the hole, a coarser mesh has been adopted to reduce the total degrees of freedom so that the computational time can be minimized. Each layup contains one element in thickness direction. Table. 2.1 shows the material properties are applied to the finite element model . The degree of freedom (dof) along x-direction is constrained on the left side of the laminate. In addition, nodes along y = 0 and z = 0 on the left side are constrained in y-direction and z -direction respectively to impose boundary conditions. The degrees of freedom along x-direction of all the nodes in the left side of the specimen is coupled together and displacement in x-direction (u) is applied at the master

18
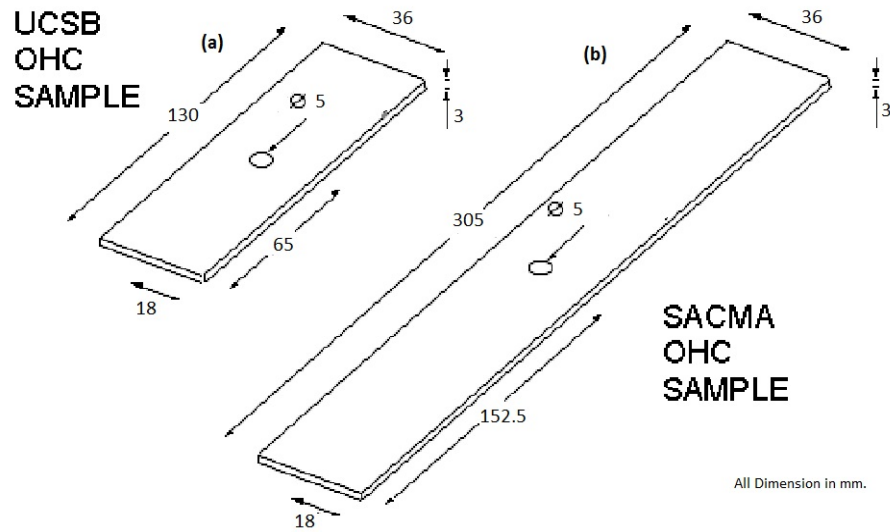
Figure 2.10: Comparison of UCSB and SACMA OHC Test Specimens
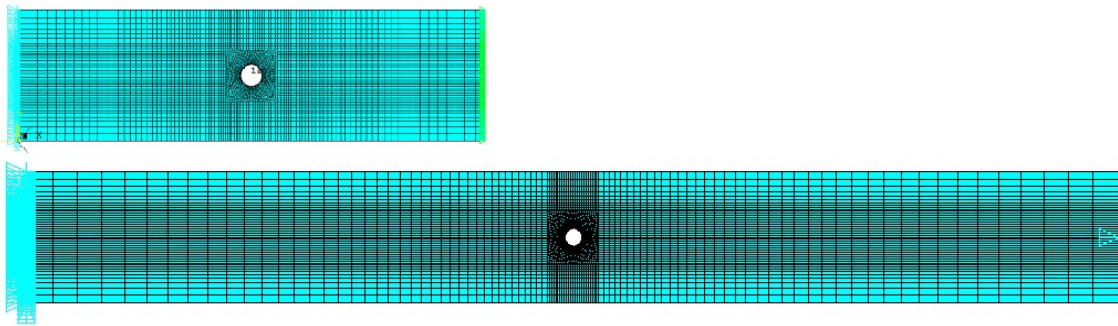
Figure 2.11: ANSYS Finite Element Analysis models of SACMA and UCSB OHC Samples

node which is located at the center of that face.

2.4.2 Experimental Specimen Preparation

The specimens are prepared from composite laminates fabricated in-house using hand layup technique. The composite laminates are made of UD carbon fiber mat (supplied by Golbond) of 230 gsm. The matrix is made from epoxy resin LY-556 mixed with hardener HY-951 (both Huntsman grade) in the ratio of 10:1 by weight. The average thickness of each layer of laminate after casting is found to be 0.375 mm. The typical geometry and dimensions of OHC specimens are shown in Fig. 2.10. A circular hole of 5 mm diameter is drilled at the center of the panel (see Fig. 2.10). The experimental setup used in the present study is shown in Fig. 2.12(a) SACMA test method and (b) UCSB test method. It consists of a computer controlled MTS Landmark servo-hydraulic cyclic test machine of

Table 2.1: Material properties of the carbon/epoxy laminate [11, 12]

Material properties	Value
Longitudinal modulus , E_{xx} (GPa)	84.16
Transverse modulus, $E_{yy} = E_{zz}$ (GPa)	7.12
Shear modulus, $G_{xy} = G_{xz}$ (GPa)	3.30
Shear modulus, G_{yz} (GPa)	2.47
Poisson's ratio (ν_{xy})	0.31
Poisson's ratio (ν_{xz})	0.43
Poisson's ratio (ν_{yz})	0.31
Longitudinal tensile strength, X_T (MPa)	1080
Transverse tensile strength, Y_T (MPa)	35
Longitudinal compressive strength, X_C (MPa)	600
Transverse compressive strength, Y_C (MPa)	90
Shear strength, $S_{xy} = S_{yz}$ (MPa)	57
Shear strength, S_{xz} (MPa)	28.5

100 kN capacity. All specimens are loaded in compression and the test is carried out in displacement control mode of 2 mm/min. The load and displacement data values are stored in user interference system from MTS for every 0.006 sec.
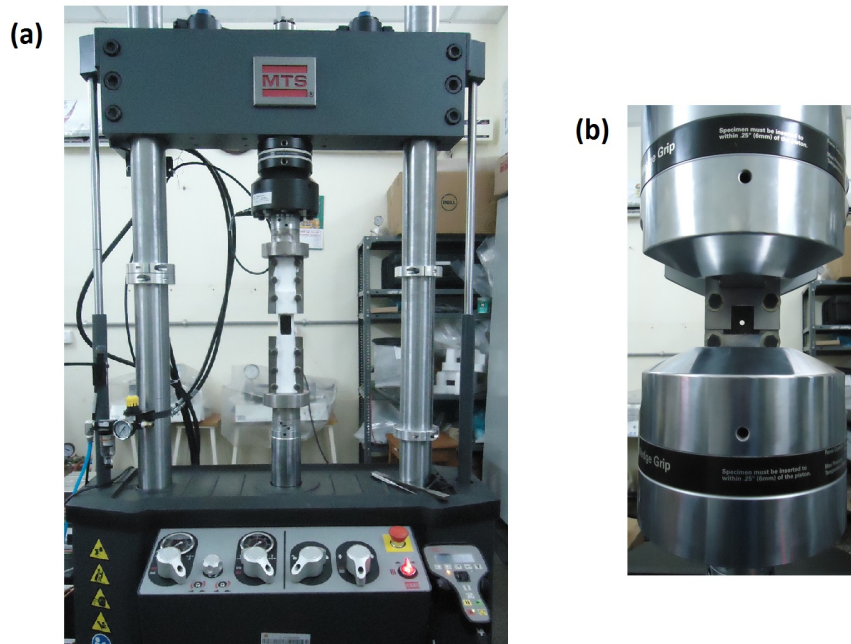
Figure 2.12: Experimental Setup (a) SACMA Test Fixture (b) UCSB Test Fixture

2.4.3   Results and Discussions

Unnotched Compression Testing with SACMA and UCSB Fixture

The SACMA and UCSB fixture have been used to test unnotched CFRP quasi-isotropic [+45/0/-45/90]$_S$ 8 layered specimens. When unnotched specimen is installed, the window in the center of the fixture can be used to view the final failure of specimen. Failure compressive stress and failure strain obtained from testing for unnotched specimen is shown as in Table 2.2.

Table 2.2: Failure Stress and Failure Strain of quasi-isotropic [+45/0/-45/90]$_S$ for SACMA and UCSB Unnotched test specimens

Specimen No.	SACMA		UCSB	
	Failure Stress (MPa)	Failure Strain	Failure Stress (MPa)	Failure Strain
1	252.77	1.431	253.43	1.123
2	265.56	1.463	250.06	1.092
3	261.81	1.472	242.24	1.076
4	257.07	1.472	245.52	1.056
Avg.	259.30	1.465	247.55	1.086
Std, Dev.	5.57	0.026	4.94	0.028
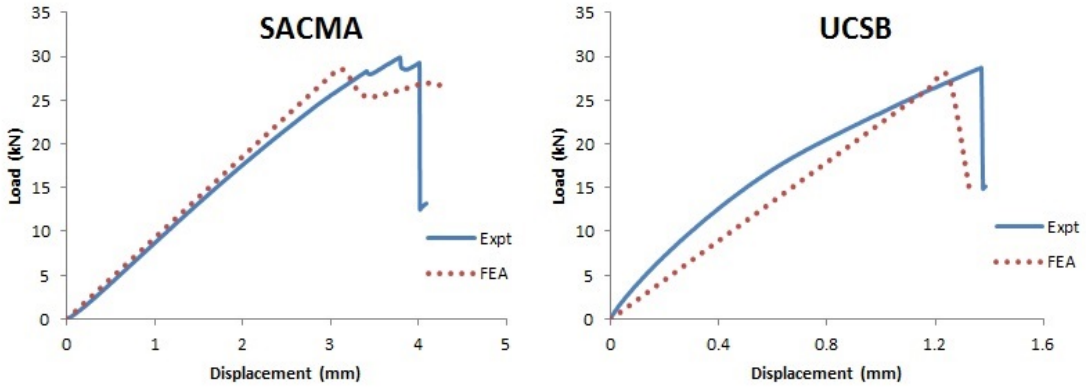
Figure 2.13: Comparison of experimental and FEA of Load Vs. Displacement curve for SACMA and UCSB Unnotched test specimens

Figure. 2.13 show the comparison of load vs. Displacement obtained from experimental and finite element analysis for SACMA and UCSB specimens. It can be observed that failure strength of quasi-isotropic specimens with both SACMA and UCSB fixture test method is approximately same i.e. 29.14 kN and 28.64 kN respectively. Whereas failure displacement for SACMA fixture test is more as compared to UCSB fixture test, since longer specimen

is used in SACMA for testing and buckling of long specimen results in more displacement in long specimen due to bigger opening window.

Open Hole Compression (OHC) Testing with SACMA and UCSB Fixture

The SACMA and UCSB fixture has been used to test unnotched CFRP quasi-isotropic [+45/0/-45/90]$_{2S}$ specimens. When an OHC specimen is installed, the window in the center of the fixture can be used to accommodate strain gauge to determine failure strain as shown in fig.1.16. Failure compressive stress and failure strain obtained from testing for OHC specimen are shown as in Table 2.3.

Table 2.3: Failure Stress and Failure Strain of quasi-isotropic [+45/0/-45/90]$_S$ for SACMA and UCSB Notched (OHC) test specimens

Specimen No.	SACMA		UCSB	
	Failure Stress (MPa)	Failure Strain	Failure Stress (MPa)	Failure Strain
1	201.80	0.925	201.59	0.832
2	203.26	0.895	205.05	0.794
3	209.25	0.906	207.68	0.812
4	206.35	0.913	211.57	0.786
Avg.	205.17	0.910	206.47	0.806
Std, Dev.	3.32	0.013	4.22	0.021
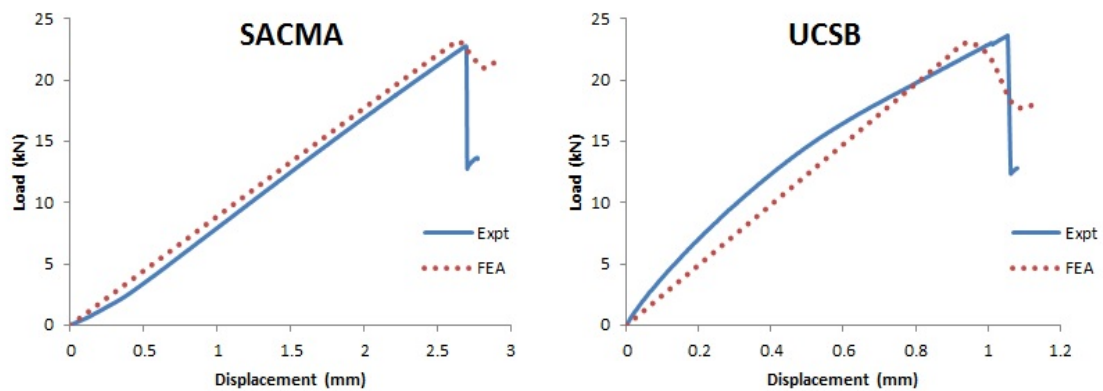
Figure 2.14: Comparison of experimental and FEA of Load Vs. Displacement curve for SACMA and UCSB OHC test specimens

Figure.2.14 show the comparison of load vs. Displacement obtained from experimental and finite element analysis for SACMA and UCSB specimens. It can be observed that failure strength of quasi-isotropic specimens with both SACMA and UCSB fixture test method is approximately same i.e. 23.15 kN and 23.63 kN respectively. Whereas failure displacement

for SACMA fixture test is more as compared to UCSB fixture test, since longer specimen plays less role since buckling is prevented and the cross-section remains the damage in both test.
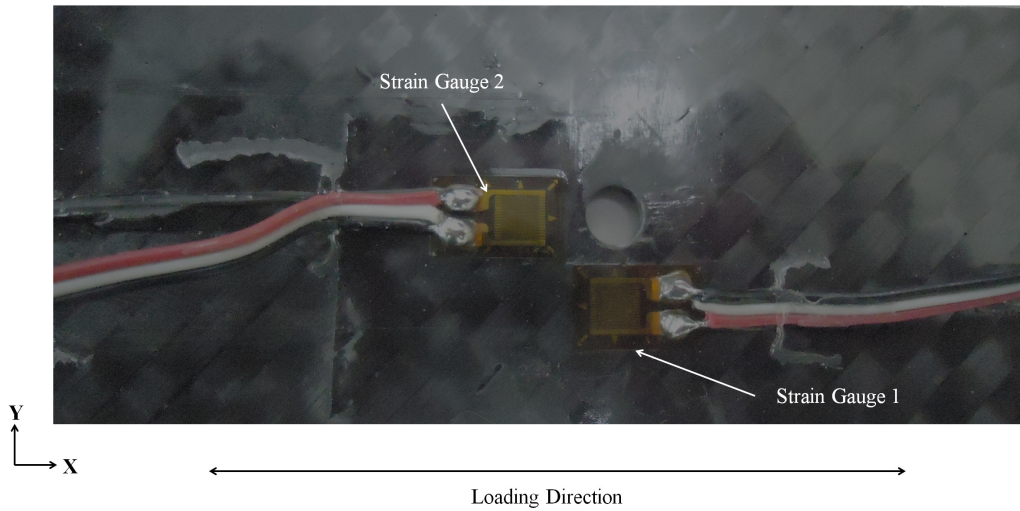
Figure 2.15: Strain Gauge Position on OHC Specimens

Experimental stress-strain curve till final damage for OHC specimen under compressive load is obtained with the help of strain gauges. During the experiment, in each specimen the data is traced at 2 different locations using strain gauge as shown in the Fig. 2.15. Strain gauge 1 is pasted at location in transverse direction at a distance of 10 mm from hole while strain gauge 2 is pasted in longitudinal direction at a distance of 15 mm from hole as shown in Fig.1.16. Longitudinal stress-strain behaviour at two specific points is plotted using the strain gauge indicator; cross and triangular markers represents for the point 1 and 2 respectively. At the same point, strain data is also obtained from FEA model till final damage and comparison between stress-strain behaviour from experiment and finite element analysis as shown in Fig. 2.16. It is observed that the point 1 data set show higher strains than that of the point 2 data because it is located near to the strain concentration zone surrounding the hole and would experience high strain gradients. It is observed that strain data from experimental and numerical data obtained from FEA shows good coherence.

2.5 Closure

Comparision between SACMA and UCSB OHC test fixture is successfully conducted. The UCSB compression test method provides consistent and accurate experimental results with compared to SACMA. However, the linearity of the load-displacement curve need to be controlled through Hydraulic Gripping pressure. The UCSB fixture can also be used in standard, smaller hydraulic grips. It does not require tabbing or necking specimen prepara-
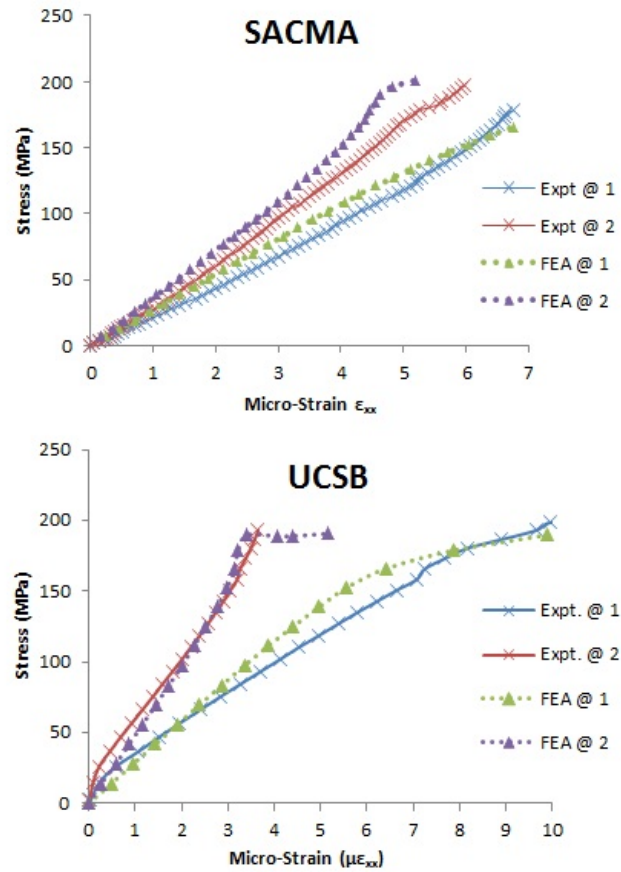
Figure 2.16: Comparison of experimental and FEA of Stress-Strain Variation for SACMA and UCSB OHC test specimens

tion that some of the other established test methods do. Its light weight facilitates specimen and fixture loading. The support ledges prevent slipping of the sample and result in secure and accurate placement of the specimen. The small coupon size reduces material costs and preparation time. This fixture is an alternate to existing fixtures that can be utilized by many industrial and university labs without the need for larger, more expensive equipment.

Chapter 3

Progressive Damage Analysis of Interacting Holes under Compression

3.1 Introduction

In this chapter, three dimensional finite element based progressive damage model (PDM) is presented for CFRP laminates having single hole and two holes in different configurations subjected to compressive loading. The developed model is suitable for predicting failure and post failure behavior of fiber reinforced composite materials. The material is assumed to behave as linear elastic until final failure. The stress values are estimated using three dimensional finite element analysis and damage prediction is done using Hashins failure criterion for unidirectional composite laminates [52]. Damage modeling is accomplished using material property degradation method (MPDM). Digital image correlation (DIC) experiment is carried out to perform whole field strain analysis of CFRP panel with different hole configurations. Whole field surface strain and displacement from finite element prediction are compared with DIC results for validation of the finite element model. A progressive damage model is developed which can predict the onset of damage, damage progression and the post failure response. Load-deflection behavior as well as path of damage progression is predicted by both PDM simulation and experiment. They are found to be in good agreement thereby confirming the accuracy of PDM implementation. The longitudinal as well as transverse spacing between hole affect greatly on the behavior of panel with multiple holes. The maximum stress value in a panel with multiple holes changes with change in spacing. The spacing thereby influences the damage process too. Effect of spacing between the holes on stress concentration factor (SCF) is also further investigated in this chapter.

3.2 Problem description

In this study, carbon/epoxy composite laminates having two holes of different configurations are considered. The panel is of $[+45/0/-45/90]_{2S}$ configuration.The specimen geometry and the test method used in this study to determine the open hole compressive (OHC) strength in CFRP composite laminates are from the recommendations from ASTM D 6484. A slight modification to the standard is considered during fabrication of anti-bucking compression test fixture (See Fig. 3.1) to conduct DIC simultaneously (See Section on Experimental strain analysis involving DIC for greater details). The length (L), width (W) and the thickness (t) of the panel are 305 mm, 36 mm and 6 mm, respectively are obtained from 350 x 350 x 6 mm panels. We choose Diameter (D) of the holes is chosen to be 5 mm. This choice of hole diameter enables ($W/D > 3.5$) to limit the edge effects. The CFRP specimens of different hole configurations as shown in Fig. 3.2 are analyzed as part of this work. Configuration 1H contains a single hole at center, 2HL contains two holes in the longitudinal direction, 2HT contains two holes in the transverse direction whereas configuration 2HD contains two holes placed in diagonal pattern at 45°. Spacing (a) is center distance between the two holes for all the configurations is kept as 12.5mm ($2.5D$) after optimization study involving FEA (explained later).

| 1. | Long Grip | 3. Short Grip |
| 2. | M8 High Tension Bolts | 4. Support Plates |
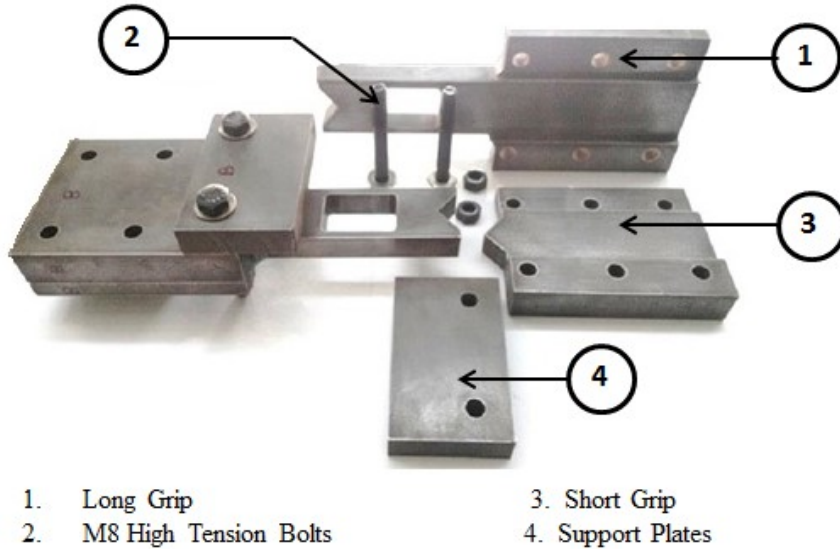
Figure 3.1: Compression Anti-Buckling Fixture (ASTM D 6484)
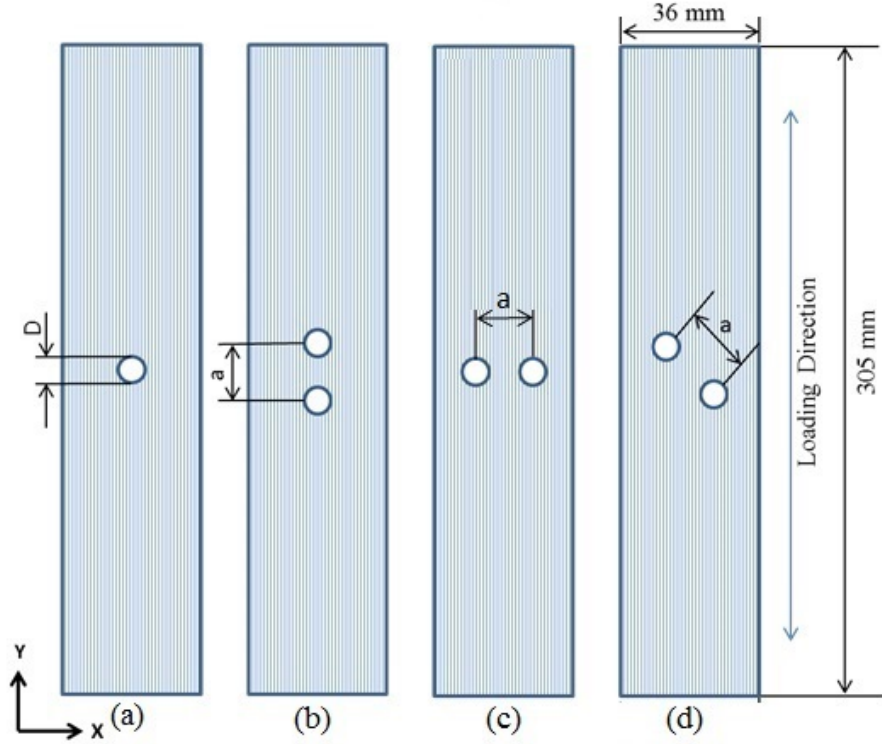
Figure 3.2: Different hole configurations (a) 1H (b) 2HL (c) 2HT (d) 2HD

3.3 Experimental Study

3.3.1 Specimen preparation

Composite laminates are fabricated by the hand layup technique with unidirectional (UD) carbon fiber mat of 230 gsm (Goldbond®). Matrix material used is a mixture of epoxy resin LY556 with hardener HY951 in the ratio of 10:1 by weight. After layup, curing is done at room temperature for 24 hrs. Once the sample is ready, specimens are cut from laminate to appropriate dimensions using abrasive cutter mounted on a hand-held saw. Later, they are machined to their exact dimensions using milling machine with carbide coated end mills at a speed of 80 rpm. Wooden backing plates are used to avoid edge delamination. Holes in the laminates are drilled in radial drilling machine with carbide coated drill bit of required diameter at a speed of 250 rpm. Wooden backing plate is used at the bottom of specimen to avoid hole-exit delamination due to drilling operation. To perform DIC experiment, random speckle patterns are made over the specimen surface. It is done by spraying GOLDEN® air brush colors (manufactured by Golden Artist Colors Inc., New Berlin, NY, USA) with Iwata CM-B airbrush (manufactured by Iwata-Medea, Inc., Portland, OR, USA) of 0.5 mm nozzle diameter. First, the specimen surface is cleaned using isopropyl alcohol. GOLDEN acrylic paint of titanium white color (#8380-Series NA) is applied over the specimen surface using

27

air brush. The white paint is allowed to dry for 1 hr. GOLDEN acrylic paint of carbon black color (#8040-Series NA) is applied over the white coated specimen surface in a random fashion using the air brush to get a random speckle pattern. Based on previous study [12], a pressure of 0.15 MPa is chosen at which adequate size and density of the black dots is obtained. An area of 100 mm^2 contains 130-150 black dots. Fig. 3.3 shows the samples of different hole configurations containing the speckle pattern.

(a)   (b)   (c)   (d)
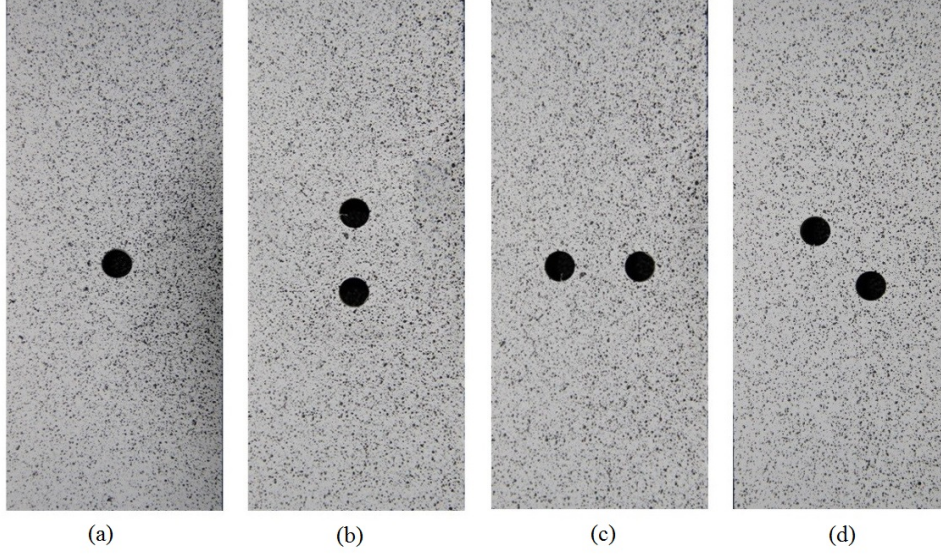
Figure 3.3: Speckle pattern applied over CFRP panel with different hole configurations (a) 1H (b) 2HL (c) 2HT (d) 2HD

3.3.2   Experimental strain analysis involving DIC

The experimental setup used for present study is shown in Fig. 3.4(a). Experiments are carried out at room temperature using an MTS Landmark® servo-hydraulic cyclic test machine of 100 kN capacity. Anti-bucking compression fixture was fabricated at Central Workshop, IIT Hyderabad as per ASTM D 6484 Standard Test Method [10]. The dimensions of the anti-bucking compression fixture are such that it prevents buckling failure and ensures only in-plane static compressive load on the specimen. Fixture has been slightly modified with window size of 40 mm long by 25 mm wide for strain analysis using DIC technique. Teflon Tape is placed on the inner walls of the fixture to reduce friction. It increases the flexural stiffness of laminate but does not carry load. Specimen with anti-buckling fixture is placed between compression platen and aligned properly as shown in Fig. 3.4(b). A 2D-DIC system (supplied by Correlated Solutions, Inc.) is used which consists of single Grasshopper® CCD Camera (POINTGREY - GRAS-50S5M-C) having a resolution of 2448 x 2048 pixels, coupled with Tamron lens (Model: SP AF 180mm F/3.5 Di). Camera is mounted on a tripod having inbuilt spirit level to ensure horizontal level.

The camera are properly aligned with respect to the specimen. Two white light emitting diode (LED) light sources (30 W capacity) are provided on both sides of the camera for ensuring proper illumination of the specimen surface. Camera is then connected to mobile workstation laptop and Vic-Snap 2009 software is used for image grabbing. Images are grabbed at predefined interval of time while applying uniaxial compression load. The test is done at a cross head speed of 2 mm/min. Load and displacement values are captured corresponding to every image being grabbed using a NI data acquisition card which interfaces image grabbing system with the MTS controller system. The test is aborted when the final failure is reached.
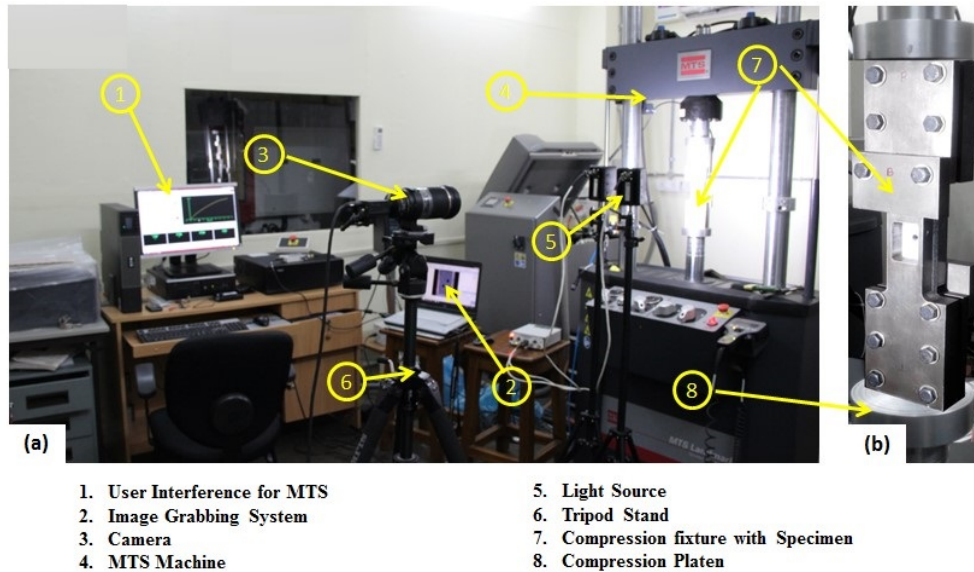
Figure 3.4: (a) Experimental Setup (b) Zoomed view of Compression Anti-buckling fixture with Specimen loaded between Compression Platen

The material properties of carbon/epoxy composite laminates used in present study are determined by conducting a series of tests as per ASTM standards. three dimensional-DIC technique is also employed for material characterization and the procedure is outlined in Ref. [11, 12, 48]. The estimated properties are given in Table 3.1.

3.4 Progressive Damage Model

Progressive damage modeling is performed based on the assumption that material shows linear elastic behavior until final failure. There are three major steps involved in PDM [12, 53, 54, 55] and they are stress analysis, damage prediction and damage modeling. Stress analysis is done by FEA involving ANSYS 13 commercial finite element package. In this step, stresses are estimated for each element in the principal material direction of the laminate. Damage prediction in composite laminates is very complicated mainly due to

Table 3.1: Material properties of the carbon/epoxy laminate [11, 12]

Material properties	Value
Longitudinal modulus , E_{yy} (GPa)	81.9
Transverse modulus, $E_{xx} = E_{zz}$ (GPa)	6.15
Shear modulus, $G_{xy} = G_{yz}$ (GPa)	2.77
Shear modulus, G_{xz} (GPa)	2.2
Poisson's ratio (ν_{xy})	0.34
Poisson's ratio (ν_{yz})	0.34
Poisson's ratio (ν_{xz})	0.3
Longitudinal tensile strength, X_T (MPa)	1300
Transverse tensile strength, Y_T (MPa)	22.97
Longitudinal compressive strength, X_C (MPa)	640
Transverse compressive strength, Y_C (MPa)	93.2
Shear strength, $S_{xy} = S_{yz}$ (MPa)	45.1
Shear strength, S_{xz} (MPa)	22.55

the presence of different failure modes or combination of them. In this study, stress based Hashins failure criterion [52] is employed for predicting damage initiation as well as damage evolution because of the following reasons. It can predict different modes of failure in a composite structure which is particularly useful for progressive damage modeling because different degradation rules need to be employed for different modes of failure. Hashins failure criteria which is basically independent of nature of loading is widely used by researchers for strength prediction as well as for progressive failure analysis. Since it is a three dimensional failure criterion, Hashins failure criteria can be adopted with three dimensional FEA study. In addition, it can be easily incorporated in ANSYS parametric development language (APDL) code. Eight sets of criteria are set for predicting eight different modes of failure. The modes of failure considered in this study are fiber failure under tensile load, fiber failure under compressive load, matrix failure under tensile load, matrix failure under compressive load, fiber-matrix shear failure in tension, fiber-matrix shear failure in compression, delamination in tension and delamination in compression. The stresses for each element and the material strength values are substituted into Hashins failure criterion for prediction of damage. Once the failure is detected in any of the elements, damage modeling needs to be done for mimicking the loss in load carrying capacity of the failed element. This is achieved by degrading the elasticity property of the failed elements and this method is termed as MPDM. When failure is detected in an element, dominant elastic material properties are degraded to 5% of their actual value according to the degradation rule given in Ref. [11, 12].

3.4.1 Finite Element Modeling

This section focuses on the development of three dimensional finite element model of the CFRP panel having cut out(s) using ANSYS 13. The panel is modelled using SOLID 186 element, which is a 20 noded brick element. The entire model contains a mapped mesh configuration. The mesh pattern surrounding the hole is kept very fine to capture the high stress gradient around it. The mesh around the circular hole has a total of 18432 elements (96 circumferential; 12 radial; 16 elements through the thickness). The number of elements along circumferential direction is chosen based on the mesh convergence study [12]. Away from the hole, a coarser mesh has been adopted to reduce the total degrees of freedom so that the computational time can be minimized. Each layup contains one element in thickness direction. For all the cases, full models are analyzed since symmetry is lost as the damage evolves. Fig. 3.5(a-d) shows the finite element model of panels with different hole configurations and Fig. 3.5(e) shows zoomed view surrounding the hole. Material properties obtained from DIC tests are applied to the finite element model (see Table. 3.1). The degree of freedom (dof) along y-direction is constrained on bottom face of the laminate. In addition, nodes along $x = 0$ and $z = 0$ on the bottom face are constrained in x-direction and z-direction respectively to impose boundary conditions. The degrees of freedom along y-direction of all the nodes in the top face of the specimen is coupled together and displacement in y-direction (v) is applied at the master node which is located at the center of that face.

3.4.2 Determining Optimal Spacing of Holes in Multiple Hole Configurations

In multiple hole configuration, interaction between the holes depend on the three important factors that are hole size, spacing between holes and type of configuration. In fact, due to the limitations of test standards on specimen width (36 mm) and to isolate the edge effects from hole to hole interactions, we keep the hole size and the spacing between the holes as constant. So we only focus on the interaction of holes based on multiple hole configurations. Hence the scope of this study is to find the influence of hole configurations on interactions.

We try to determine the optimal spacing of hole in multiple hole configuration subjected to uniaxial compression test solved using FEA. Fig. 3.6 illustrates the effect of hole spacing on stress concentration factor (SCF) for panels with different hole configurations when subjected to uniaxial compression as shown in the Fig. 3.5(a-d). It can be seen that for 2HL configuration, SCF increases as the hole spacing (a) increases. This is because as the hole spacing decreases, the ineffective region of the laminate which do not carry any load increases and the stress flux redistributes within this zone. For example, Fig. 3.7 shows the schematic of 2HL configuration showing the shielding effect with aspect ratio for the elastic homogeneous solid. Therefore, there is a shielding effect and the stress flux lines are
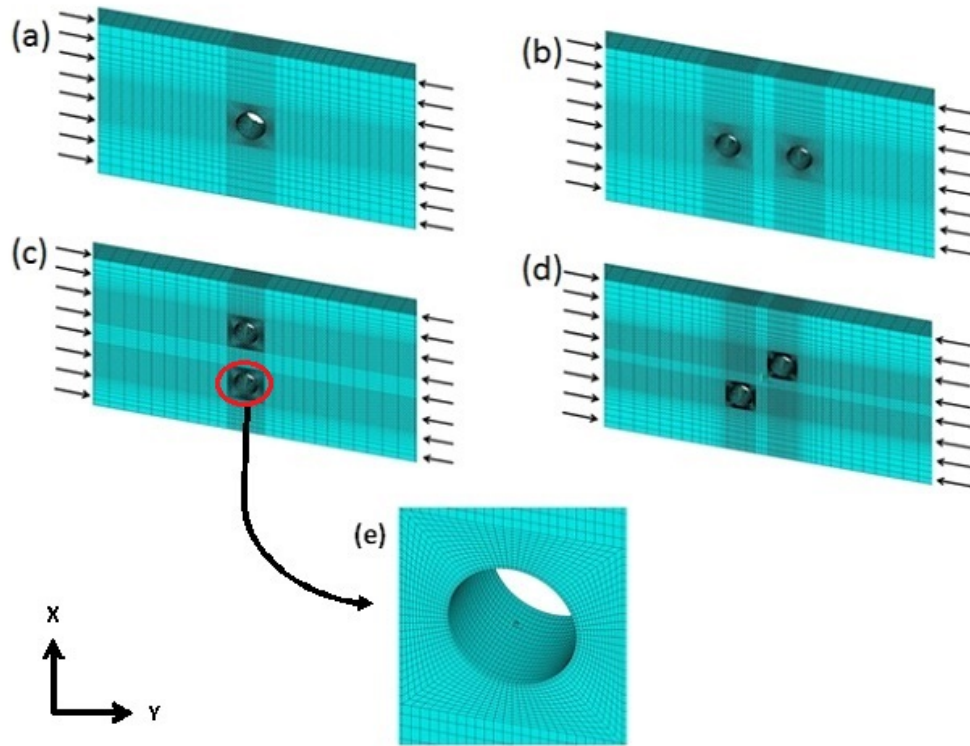
Figure 3.5: Finite element model for panels having different hole configurations (a) 1H, (b) 2HL, (c) 2HT and (d) 2HD (e) Zoomed view of the finite element model around the hole
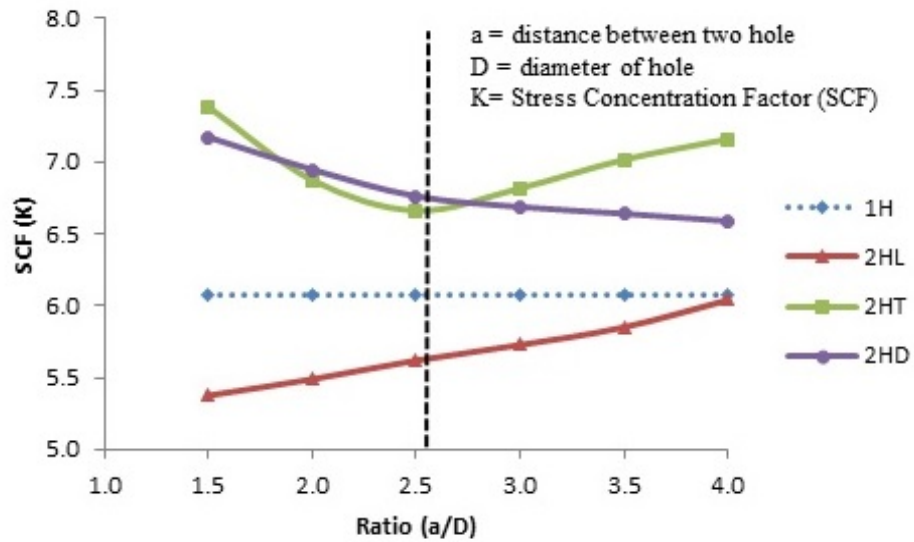
Figure 3.6: Effect of hole spacing on SCF in panel having hole configuration 2HL, 2HT and 2HD.

diverted away from the hole when they are closer. Therefore a closer spacing of holes is preferred in this configuration. On increasing the hole spacing ($a/D > 4$), SCF for 2HL configuration asymptotes to that of single hole (1H) configuration. For 2HT configuration, stress interaction between two holes becomes more severe when holes are placed closer to each other (see Fig. 3.6). As hole spacing (ST) increases from $1.5D$ to $2.5D$ (where D is the diameter of hole), SCF keeps on reducing. But for hole spacing greater than $2.5D$, it is observed that SCF increases because of increasing stress interaction between hole edge and free edge. Optimum spacing where SCF becomes least is found to be $2.5D$ in this case. In case of panel having 2HD configuration, as hole spacing increases, SCF keeps decreasing because of the lesser stress interaction between two holes (see Fig. 3.6). Thus, the limited experimental study for the range of configurations considered indicates an optimal spacing between $2D$ and $3D$. In the present study, optimum hole spacing of $2.5D$ is chosen as an average of the two.
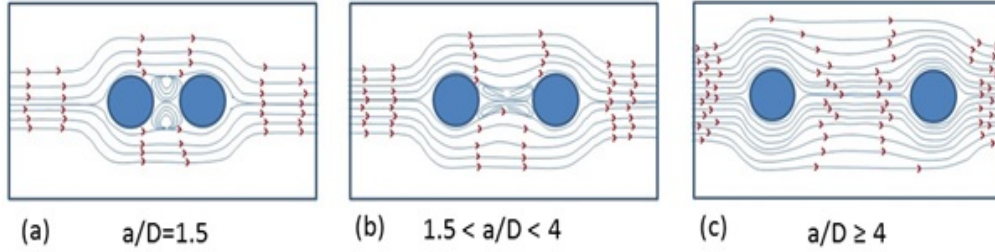
Figure 3.7: Schematic representation of stress lines variation with increasing a/D aspect ratio for 2HL configuration in elastic homogeneous solid.

3.5 Results and Discussions

3.5.1 Virgin specimens

For comparison the multi-directional compressive strength of the $[+45/0/\text{-}45/90]_{2S}$ CFRP laminate of both virgin and single hole specimen is presented in Table 3.2. It can be seen that the compressive strength of the single hole specimen is about 70% of the virgin specimen and the failure strain is less by 30% after testing three specimens each. The typical load vs. displacement behavior of both virgin and single hole specimens are plotted in Fig. 3.8. Solid line shows the load vs. displacement for the virgin specimen and the dashed line shows for single hole specimen (1H).We observe that the failure load is for the 1H specimen is much less than the virgin specimen. The final failure surface in 1H specimen is shown in Fig. 3.9. It can be seen that the failure occurs by out of plane micro-buckling of the fibers along the net section. Further, we observe that the order of decreasing compressive strength for different hole configurations are 1H, 2HL, 2HT and 2HD respectively as shown

in Table 3.2.

Table 3.2: Compressive Strength of for different hole configuration

Configuration	Compressive Strength (kN)	Failure Strain (%)
Virgin Specimen	68.73±2.65	1.35±0.04
1H	48.82±1.43	0.92±0.02
2HL	45.30±1.24	0.85±0.015
2HD	43.12±1.35	0.80±0.012
2HT	39.95±1.28	0.76±0.018
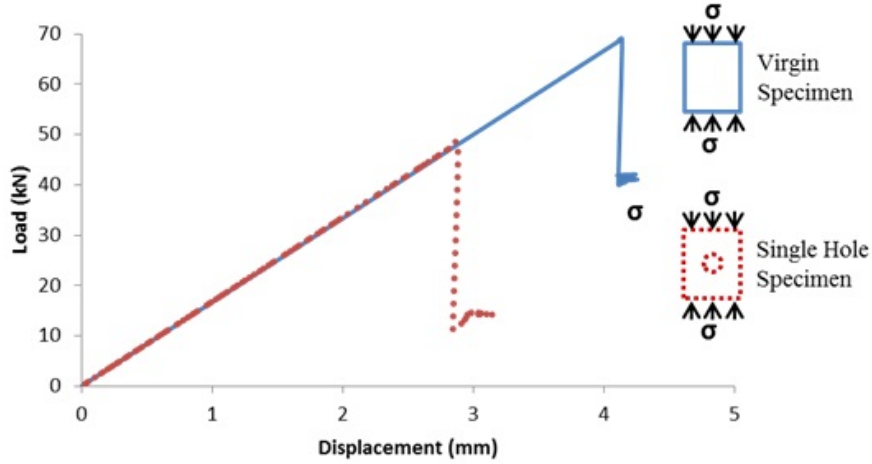
Figure 3.8: Load Vs. Displacement curve for virgin and single hole Specimen

3.5.2 Finite Element Model Validation

To validate the finite element model, whole field surface strains from FEA is compared with those from DIC experiment. Whole field strain distribution from DIC experiment is obtained for the region enclosed by the opening in the anti-buckling fixture. In Fig. 3.10(a-d) we compare the whole field ϵ_{yy} strain contour distribution obtained from both DIC and FEA for 1H, 2HL, 2HT and 2HD configuration respectively at 30 kN. All the four configurations are within the elastic limit (see Table 3.2) for 30kN compressive load. Whole field strain distribution plotted in Fig. 3.10, shows a reasonably good coherence between DIC and FEA predictions.

Further, to carry out detailed validation of FEA vs. DIC, we plotted the profile variation of whole field strain along the section AB as shown in Fig. 3.11 inset for the 2HL configuration at 30kN compressive load from both DIC and FEA. It can be observed that a close quantitative agreement exists between FEA and DIC strain data at the critical cross

34
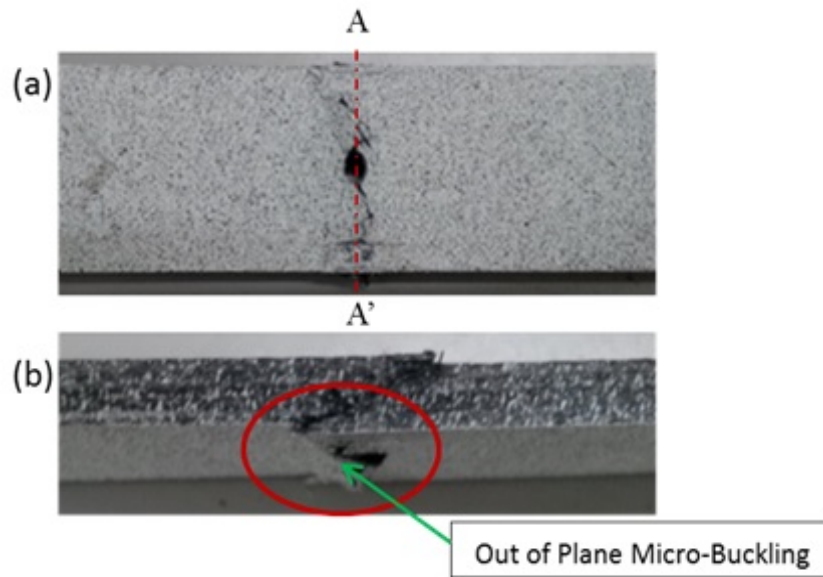
Figure 3.9: Final Failure within specimen gauge length for 1H configuration (a) Front View (b) Side view
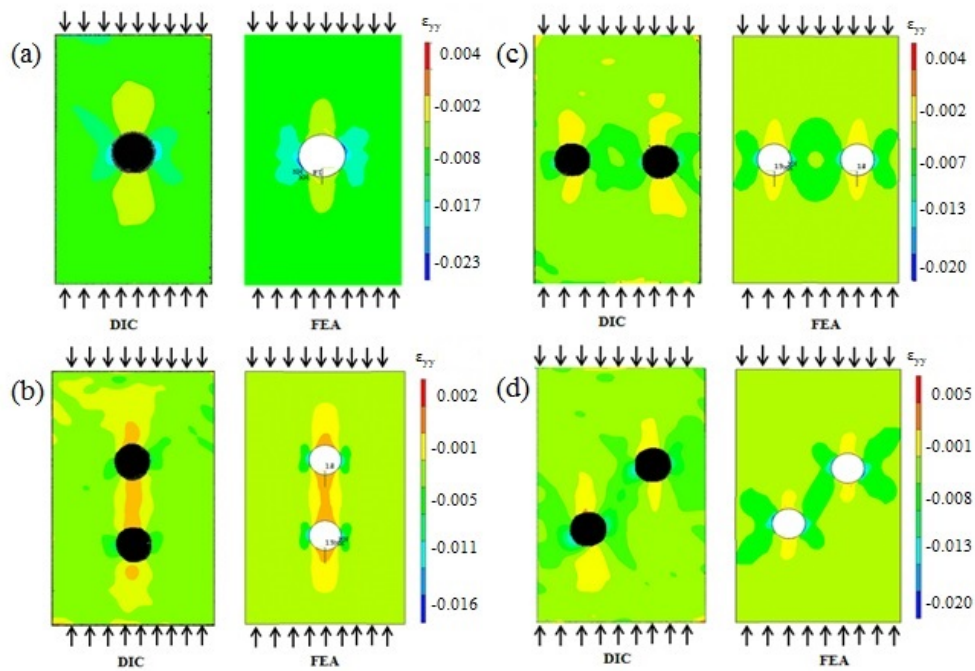
Figure 3.10: Whole Field yy strain distribution contour in the panel having configuration at 30 kN (a) 1H (b) 2HL, (c) 2HT and (d) 2HD.

section AB. Similarly, the whole field displacement in the y direction is shown for qualitative comparison between FEA and DIC results in Fig. 3.12. Even in the comparison of whole

field displacements, we observe remarkably good agreement between FEA and DIC thereby strengthening the validation of the finite element model.
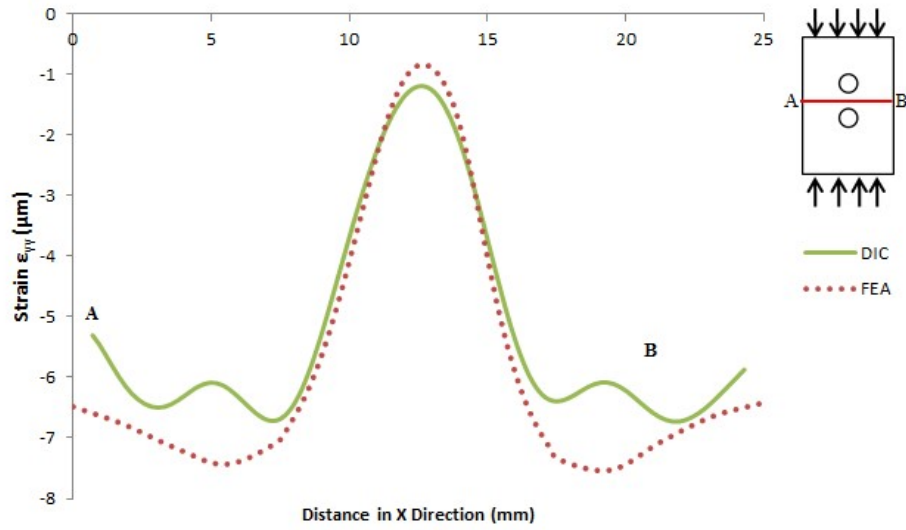
Figure 3.11: Strain Variation yy from one edge to other edge of the window for the panel having 2HL configuration at a load of 30 kN (Compression)
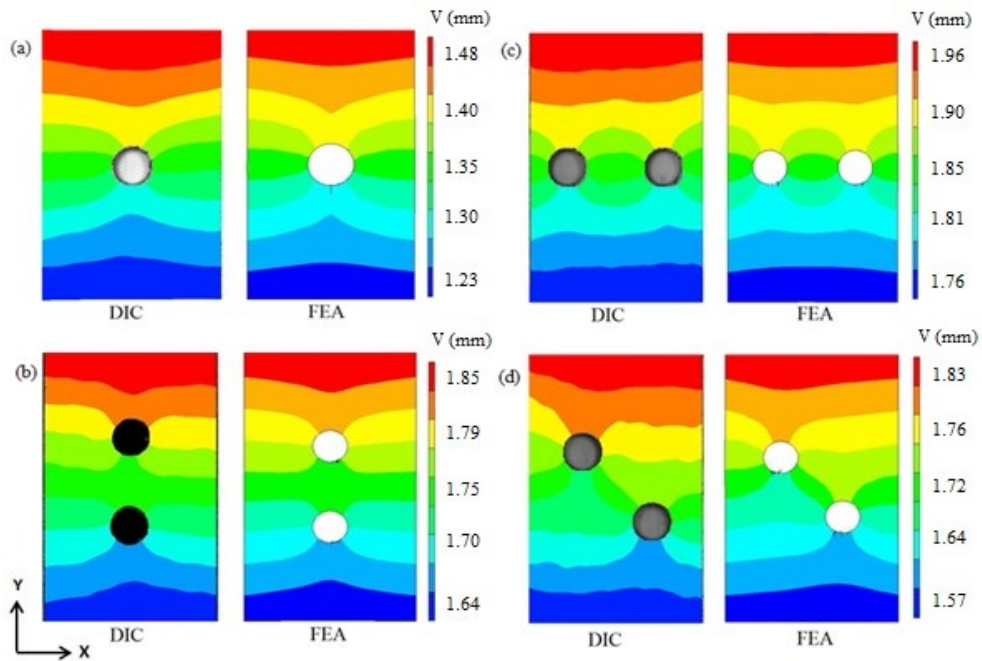
Figure 3.12: Whole field V-displacement for panel with different hole configuration (a) 1H (b) 2HL, (c) 2HT and (d) 2HD.

3.5.3 Experimental Analysis using DIC technique

Specimen with a Single Hole (1H Configuration)

In this section, experimental stress-strain curve till damage for single hole CFRP laminate under compressive load is presented. Three 1H specimens with a 5 mm diameter hole were tested to determine their failure loads. Failure in these specimens occurs along the net section AA' in a transverse direction to the loading axis, further much of the delamination and fiber micro-buckling are concentrated near hole and little damage is observed away from the hole as shown in Fig. 3.9. During the experiment the whole strain field is obtained through DIC technique till the specimens fail. Particularly, in each specimen the data is traced for three different locations as shown in the Fig. 3.13 inset. Selection of these points are as follows, point 1 is chosen far away from hole, point 2 and 3 are chosen on the section AA' such that they are 10 mm and 2 mm away respectively from the hole edge on the section AA'. Longitudinal stress-strain behavior at three specific points (location) are plotted using the strain data from DIC; circular, cross and triangular markers represent for the point 1, 2, and 3 respectively. It is observed that the point 3 data set show higher strains than that of the point 2 data because it is located near to the strain concentration zone surrounding the hole and would experience high strain gradients. Further, using regression analysis linear polynomials are fitted to the point 1 data set. The slope of the linear fit and the regression coefficient for the point 1 data set are 81.101MPa and 0.9914 respectively as shown in Fig. 3.13. Location of point 1 is far away from the hole, hence we observe that slope of the stress-strain curve at location 1 is found to be in close agreement with the Youngs modulus (ϵ_{yy}) value of the CFRP laminate as anticipated as shown in Table 3.1.
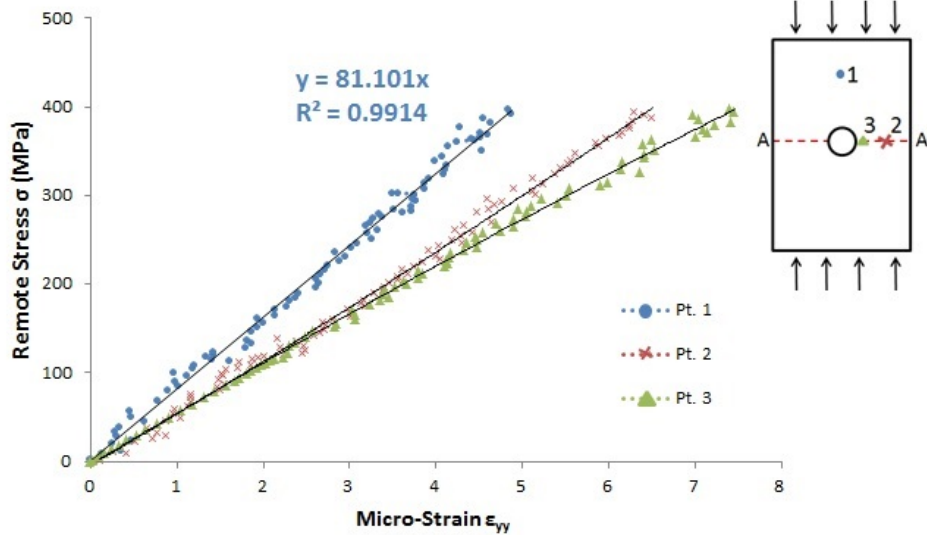
Figure 3.13: Compressive stress/strain response of specimen with one hole (d = 5 mm)

Specimens with multiple hole configuration

In this section, experimental stress-strain curve till damage for various multiple hole CFRP laminates under compressive load are presented. Three specimens are tested for every configuration having 12.5 mm (2.5 D) spacing between holes. From the series of experiment conducted, it can be concluded that specimen of 2HL configuration sustains more compressive load as well as higher failure strain as compared to 2HD and 2HT configurations respectively (see Table 3.2). In Fig. 3.14(a-c) we present the final failure specimens of 2HL, 2HT and 2HD configurations respectively. It is observed that in 2HL and 2HT configurations, fiber buckles at the edges of holes and final failure occurs transverse to the loading direction at the net section as shown in Fig. 3.14(a-b). Whereas, in 2HD configuration fiber buckles at edge of the holes but progresses diagonally first and intersects the two holes before continuing transverse to the loading direction as shown in Fig. 3.14(c). Further, we also observe that, in case of 2HL configuration, final failure occurs around one hole while in other configurations, final failure occurs around both the holes.
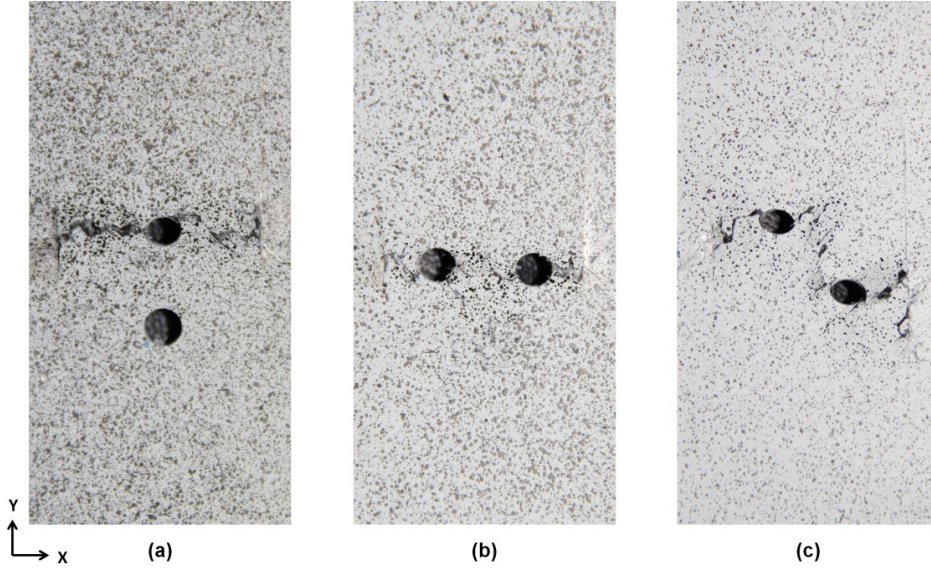
Figure 3.14: Multiple hole final failure (a) 2HL (b) 2HT (c) 2HD

During the experiment the whole strain field is obtained through DIC technique till the specimens fail. Particularly, in each specimen the data is traced for three different locations and plotted as shown in the Fig. 3.15(a-c). Selection of these points is as follows, point 1 is chosen far away from hole, point 2 is chosen at center between two hole and point 3 is chosen 2 mm away from the hole edge on a transverse line joining the closest boundary to the loading direction for all the three configurations as shown in Fig. 3.15(a-c) insets. Longitudinal stress-strain behavior at 3 specific points (location) is plotted using the strain data from DIC; circular, cross and triangular markers represent for the point 1, 2, and 3

respectively for configurations 2HL, 2HT and 2HD separately in Fig. 3.15(a-c) . For all the three configuration shown in Fig. 3.15, at location 3 higher strain levels are seen compared to that of the location 1 and 2 because it is situated nearer to the hole edge where stress concentration is higher. Whereas at location 2, 2HL configuration shows lesser strain as compared to configuration 2HT and 2HD. This is because two holes are present along the loading direction providing shielding effect at location 2 as the stress flux lines are deflected resulting in a lower stress. Further, using regression analysis linear polynomials are fitted to the point 1 data set. The slope of the linear fit for the point 1 data set are 81.18 MPa, 81.25 MPa, and 81.32 MPa for 2HL, 2HT and 2HD configuration respectively as shown in Fig. 3.15(a-c). In all these configurations location of point 1 is far away from the hole, hence we observe that slope of the stress-strain curve at location 1 is in close agreement with the Youngs modulus (ϵ_{yy}) value of the CFRP laminate as anticipated as shown in Table 3.1.
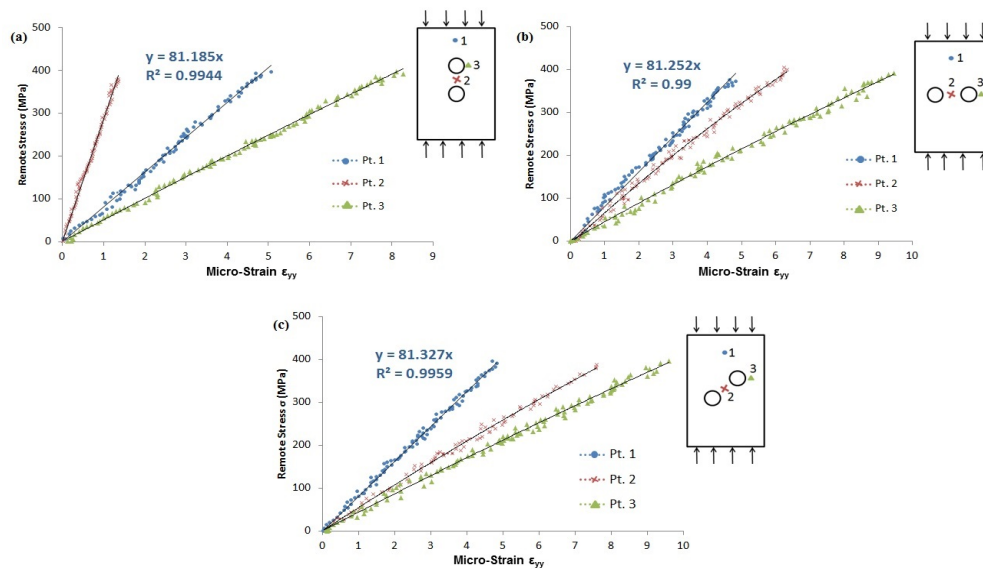
Figure 3.15: Compressive stress/strain response of specimen for condition (a) 2HL, (b) 2HT and (c) 2HD (a/D =2.5).

3.5.4 Progressive Failure Analysis

Load-displacement curves predicted by PDM simulations for composite panels for 1H, 2HL, 2HT and 2HD configurations are compared with the corresponding experimental behavior as shown in Fig. 3.16(a-d) respectively. The load-displacement behavior from PDM closely matches with the experimental one. It is to be noted that a good agreement exists in case of load values whereas displacement is under-predicted by FEA.Longitudinal stress-strain behavior away from the holes is plotted for all the three panel configurations from both PDM and DIC. They are shown in Fig. 3.17 (a-h) Slope of the stress-strain curves obtained

from PDM and DIC are found to be in close agreement with the Youngs modulus (E_{yy}) value of the composite laminate once again confirming the accuracy of PDM algorithm developed. The choice and implementation of composite failure theory is very critical in the accuracy of PDM prediction. Several composite failure theories perform well in specific cases and poor in others [56], suggesting trial and error basis for selection. Besides this, there are approximations involved in the material property degradation rules as well as in the degradation factors. The above mentioned factors could be the reason for deviation between PDM and DIC results shown in Fig. 3.16. In Table 3.3 we present failure initiation load (obtained through FEA), at which failure starts (from any mode) in any of the element in the panel predicted by PDM. Further, the ultimate load (load at final failure) predicted from both experiments as well as PDM are also tabulated in Table 3.3. It is observed that composite laminate with two holes in longitudinal direction (2HL) sustains highest load before final failure compared to the other two configurations (2HT and 2HD). Usually there is a significant amount of damage accumulation around the hole due to fiber-matrix shear failure, matrix failure, delamination due to both tension and compression. Damage typically initiates from the hole edge and propagates towards the transverse free edge along the net section. Further, we observe that the order of decreasing failure initiation load for different configurations is 2HL, 1H, 2HD and 2HT. It is expected that the 2HD initiation is somewhere in between 2HT and 2HL. Whereas, it is to be noted that 2HL has higher than 1H, because as discussed earlier the holes in 2HL experience shielding effect hence the SCF in 2HL is lower than 1H for $a/D = 2.5$ as shown in Table 3.3. Hence the failure initiation load for the 2HL is greater than 1H configuration. However, this shielding effect doesn't influence the ultimate compressive strength, since the overall stiffness for 2HL is lower than that of 1H, hence ultimate compressive strength for 1H is greater than 2HL as shown in Table 3.3. Among multiple hole configuration, 2HL is preferred since it has got higher initiation and final failure load.

Table 3.3: Failure initiation and ultimate load ($a/D = 2.5$)

Configuration	Failure Initiation Load (kN)	Ultimate Load (kN)	
		Experiment	PDM
1H	11.85	48.82±1.43	46.43
2HL	12.74	45.30±1.24	43.30
2HT	9.08	39.95±1.28	38.72
2HD	9.99	43.12±1.35	41.50

Fig. 3.18 shows the PDM prediction of failure initiation zones around the typical hole edge. For all the configurations studied, matrix failure is the first mode of failure initiation followed by the fiber-matrix shear failure and they are in line with the observation in literature [39, 40]. Figs. 3.19-3.22 shows detailed illustrations predicted for plywise damage
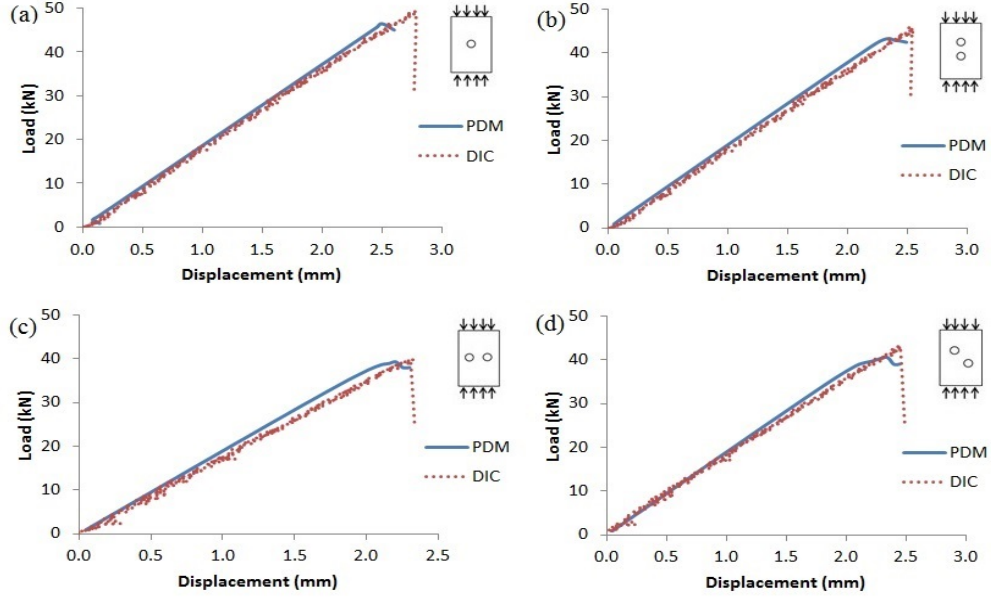
Figure 3.16: Load-displacement behavior for panel with different hole configurations (a) 1H (b) 2HL, (c) 2HT and (d) 2HD.

progression in a $[+45/0/-45/90]_{2S}$ laminate for 1H, 2HL,2HT and 2HD configurations respectively at different load levels. Damage typically initiates from the hole boundary, where the stress concentration is higher. Plywise failure initiation load predicted by PDM for all configurations, are tabulated in Table 3.4.

Table 3.4: Plywise failure initiation load (kN)

Configuration	+45°	0°	-45°	90°
1H	16.42	11.85	16.62	22.78
2HL	17.29	12.74	17.29	25.46
2HT	14.53	9.08	14.53	20.87
2HD	15.43	9.99	15.43	22.67

Fig. 3.19 illustrates the progressive damage in $[+45/0/-45/90]_{2S}$ laminate having single hole (1H configuration) with increasing load. In 0° layers, matrix failure and fiber-matrix shearing failure initiate near the hole at a load of 11.85 kN followed by delamination as the damage grows with load. Fiber-matrix shear failure and matrix failure initiate near the hole edge in ±45° layers at a load of 16.42 kN. Later, in 90° layers, delamination in compression along with matrix failure initiate near the hole edge at a load of 22.78 kN followed by delamination in tension as load increases. Damage mostly grows in the direction normal to the loading direction. Finally, as the load approaches a value of 46.43 kN, the damage propagates very rapidly normal to the loading direction from the transverse hole
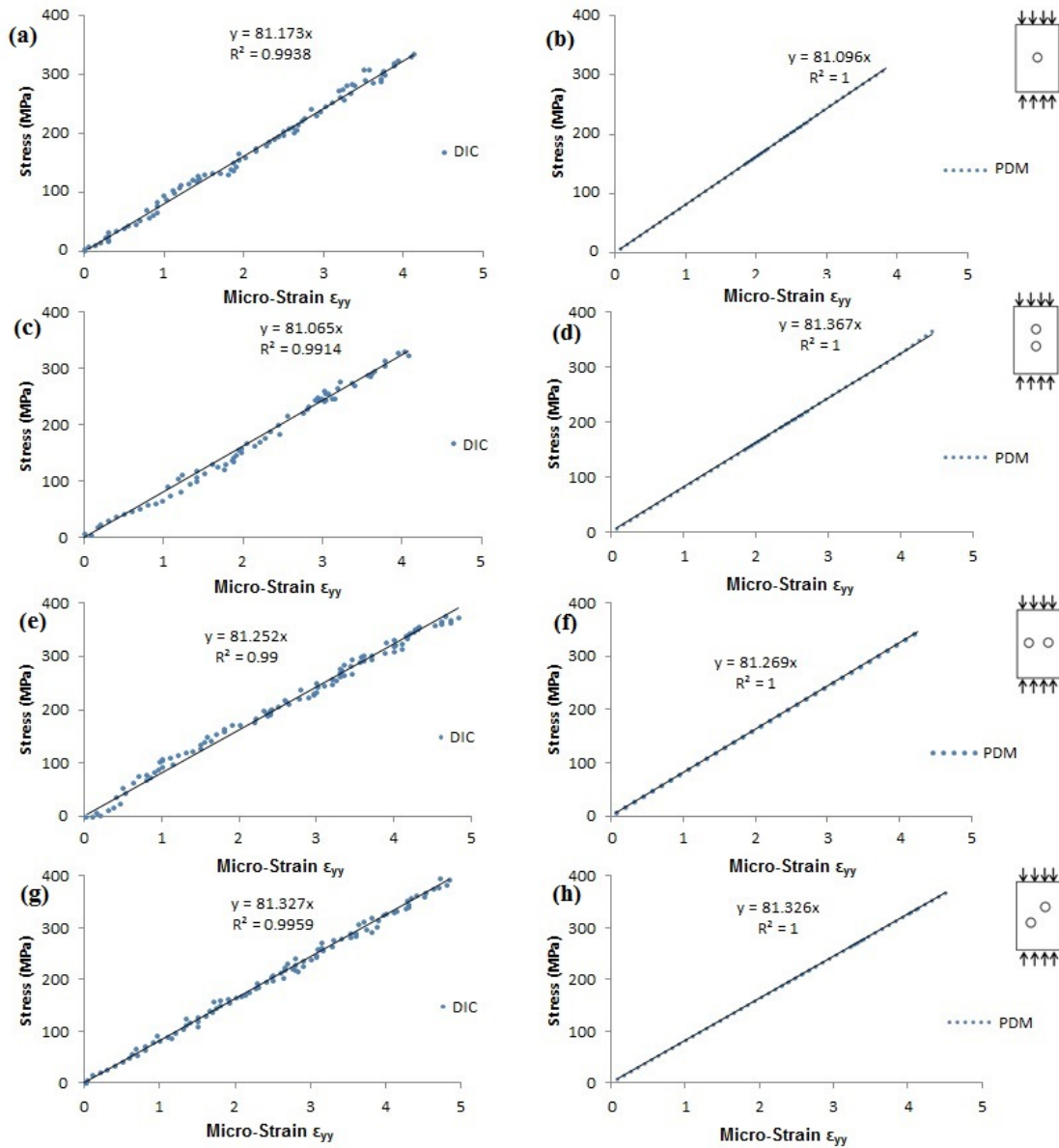
Figure 3.17: Stress-strain curve for different panel configurations far away from hole (a) for 1H configuration from DIC (b) for 1H configuration from PDM (c) for 2HL configuration from DIC (d) for 2HL configuration from PDM (e) for 2HT configuration from DIC (f) for 2HT configuration from PDM (g) for 2HD configuration from DIC (h) for 2HD configuration from PDM

edge towards free edge of the laminate, resulting in the total failure along the net section as shown in Fig. 3.23(a).

Figs. 3.20-3.22 illustrate the progressive damage in the laminate having different hole configurations with increasing load. In general for all multiple hole configurations, in 0° layer damage gets initiated by matrix failure followed by fiber-matrix shearing failure around the
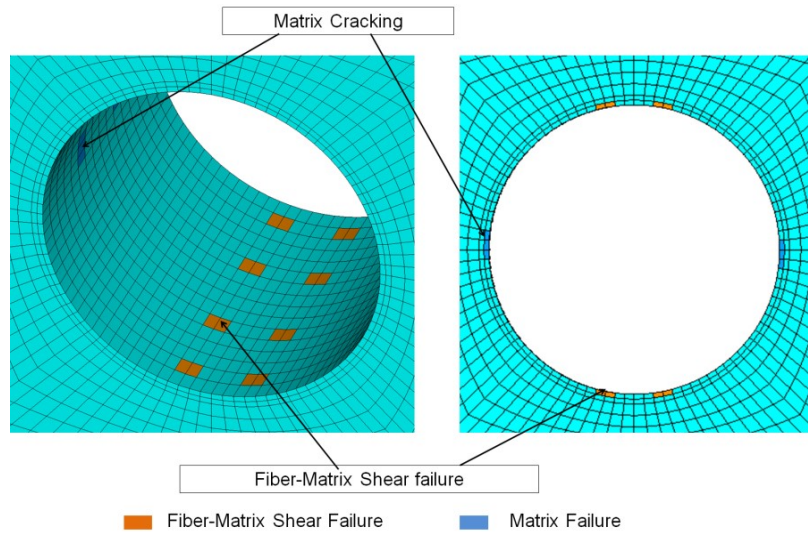
Figure 3.18: Damage initiation site in the 0° layer around the hole in an open cutout quasi-isotropic panel (+45/0/-45/90)2S during compression loading

hole edge. Subsequently, delamination develops as the load level increases. At higher loads, ±45° layers initiate failure, the failure modes are mainly dominated by the fiber-matrix shear along with matrix failure. In addition, delamination occurs at hole edge over small region. On further increase in load, delamination along with matrix failure near the hole edge gets intiated in 90° layers. Overall, the final failure mechanism observed on +45° layer (surface) from experiment is in good coherence with the PDM prediction as shown in Fig. 3.23(b-d) thereby confirming the accuracy of the developed damage model.

3.6 Closure

In this work, a three dimensional finite element based PDM is developed for composite laminates having two holes of different configurations subjected to in plane compressive load. Hashins failure criteria is used for damage prediction and MPDM is implemented for damage evolution. Finite element model is first validated by comparing whole field surface strains and displacements obtained from FEA with those from DIC experiment. They are found to be in good coherence. For first time in literature, here shown the application DIC technique for compression study of open hole(s) specimens. DIC is found to be reliable and accurate for such study and is recommended. The PDM algorithm is implemented to predict different modes of failure, load-deflection behavior and damage progression up to final failure for panel different hole configurations. Further, Load-deflection behavior predicted by PDM is compared with the experimental behavior and is found to be in good agreement. Among various multiple hole configurations studied, the 2HL laminate has sustained maximum load of 45.30 kN which is 11.8% and 4.8% more than that of 2HT and 2HD configurations,

Figure 3.19: Illustration of damage propagation predicted by the PDM with increasing load for $[+45/0/-45/90]_{2S}$ laminate having 1H configuration.

respectively. For all the hole configurations, damage initiates in $[0°]$ layers as fiber-matrix shear failure and matrix failure at hole edges and it progresses in the transverse direction towards free edge at the net section. The damage mechanism predicted by PDM is also in good coherence with the experimental observations there by confirming the accuracy of the PDM algorithm developed. The results of the damage propagation predicted by the model shows that the majority of the damage in case for open hole composite laminates under compressive load is fiber-matrix shear failure, matrix failure and delamination. Eight failure modes observed are coupled to one another, hence initiation of one failure mode of damage induces other failure modes of damage subsequently leading to final failure. For all

44
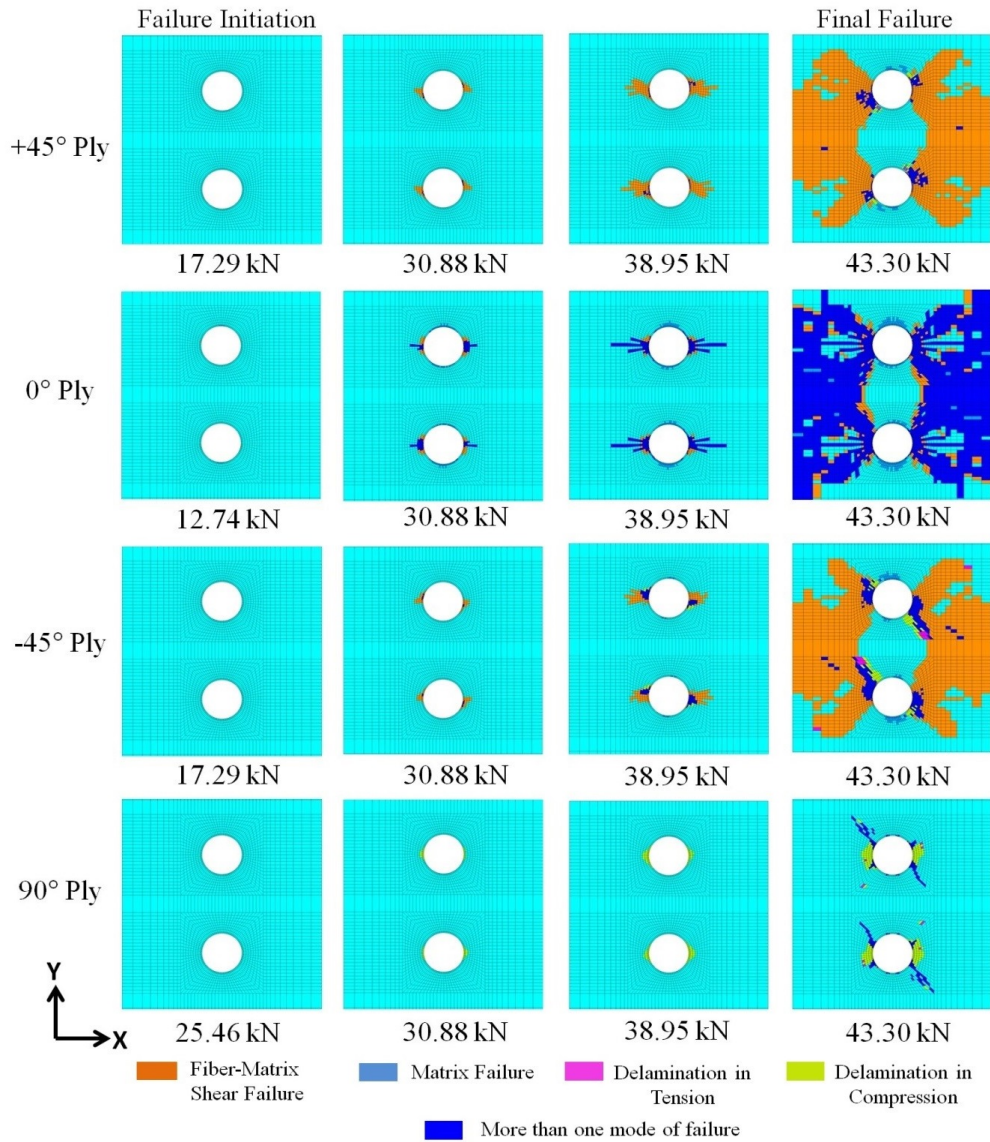
Figure 3.20: Illustration of damage propagation predicted by the PDM with increasing load for $[+45/0/-45/90]_{2S}$ laminate having 2HL configuration.

the three configurations, hole-hole interaction ceases when the spacing exceeds four times the hole diameter and starts to behave like single hole specimen. Based on the FEA study, a/D ratio of 2.5 is recommended for multiple hole configurations resulting in lower SCF and it is the same for tensile load behavior as well (Ref. [11]). Among multiple hole configuration, 2HL is preferred since it has got higher initiation and final failure load.
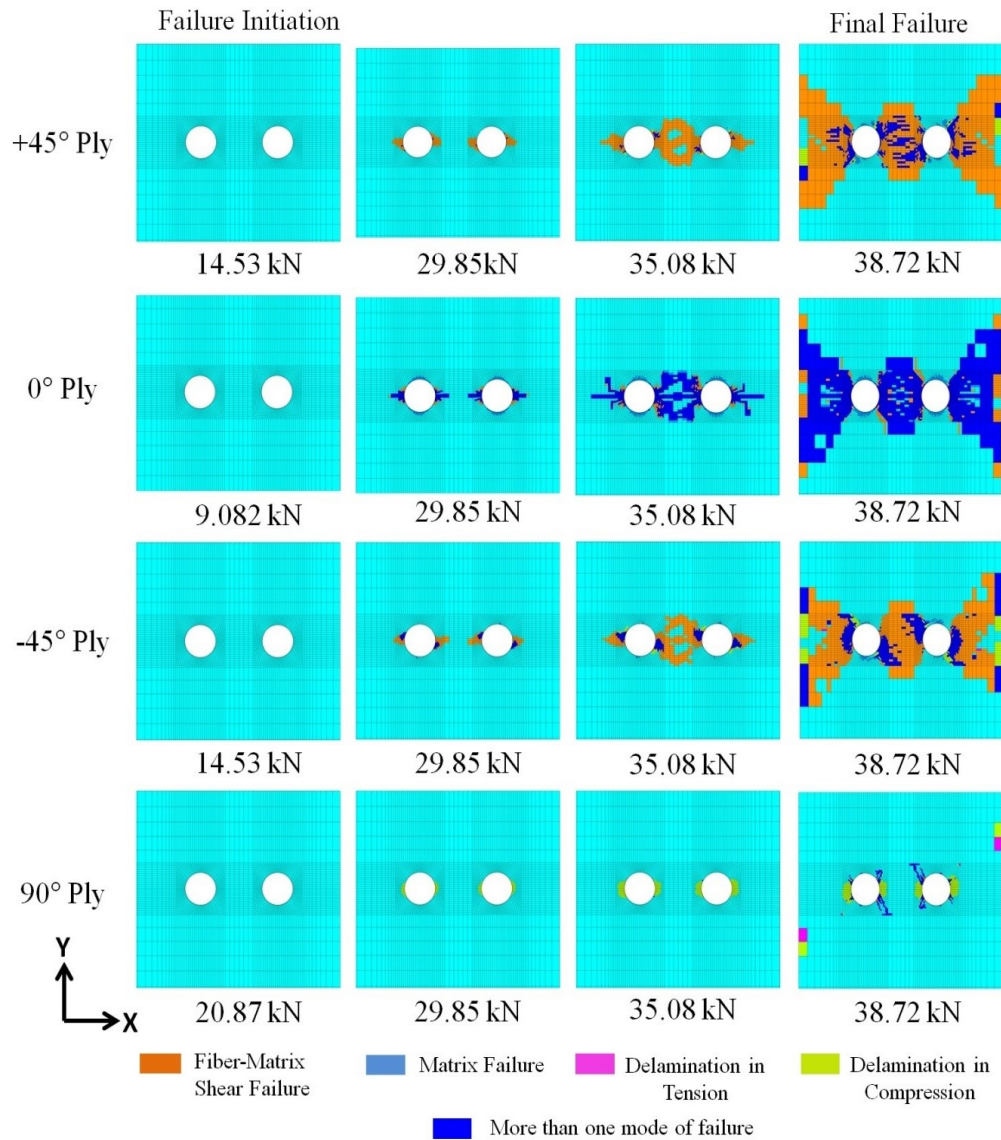
Figure 3.21: Illustration of damage propagation predicted by the PDM with increasing load for $[+45/0/-45/90]_{2S}$ laminate having 2HT configuration.
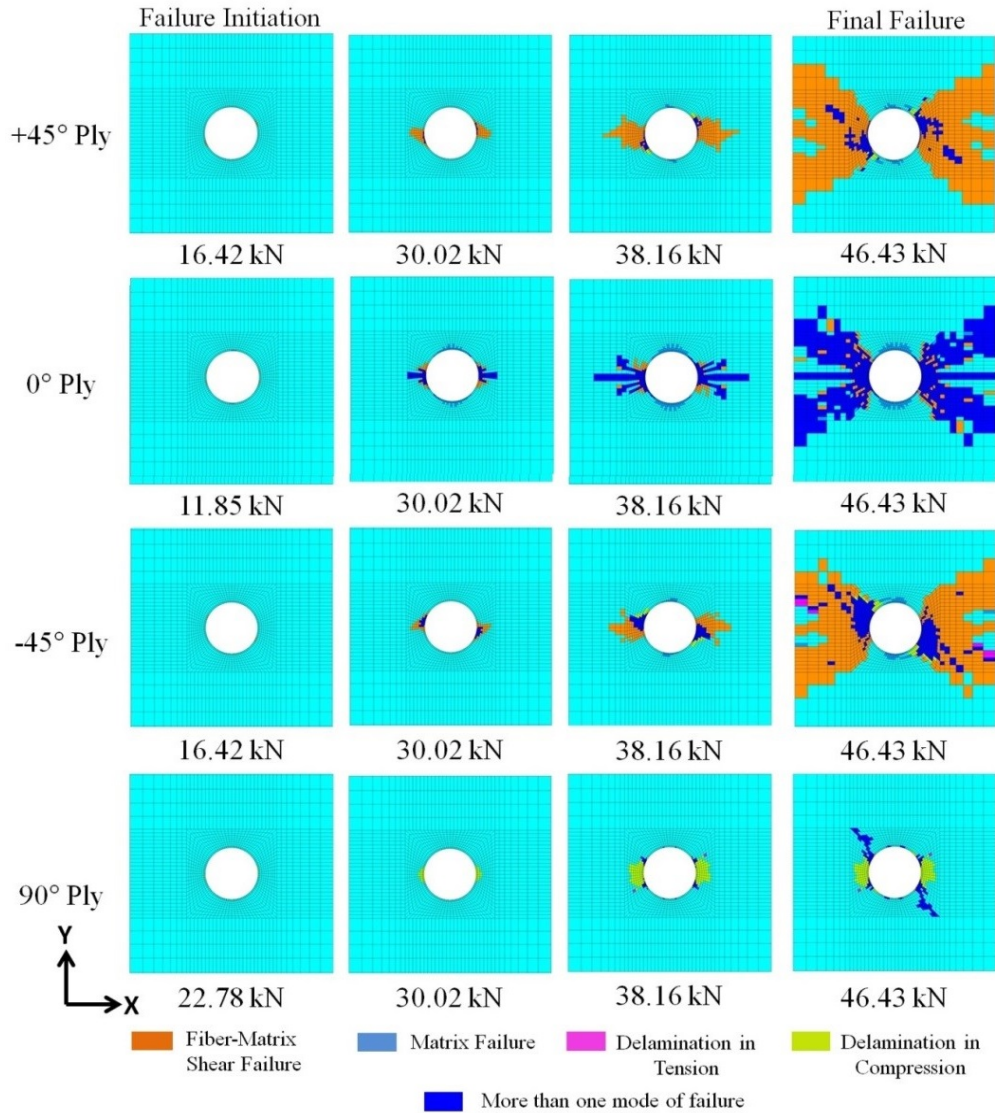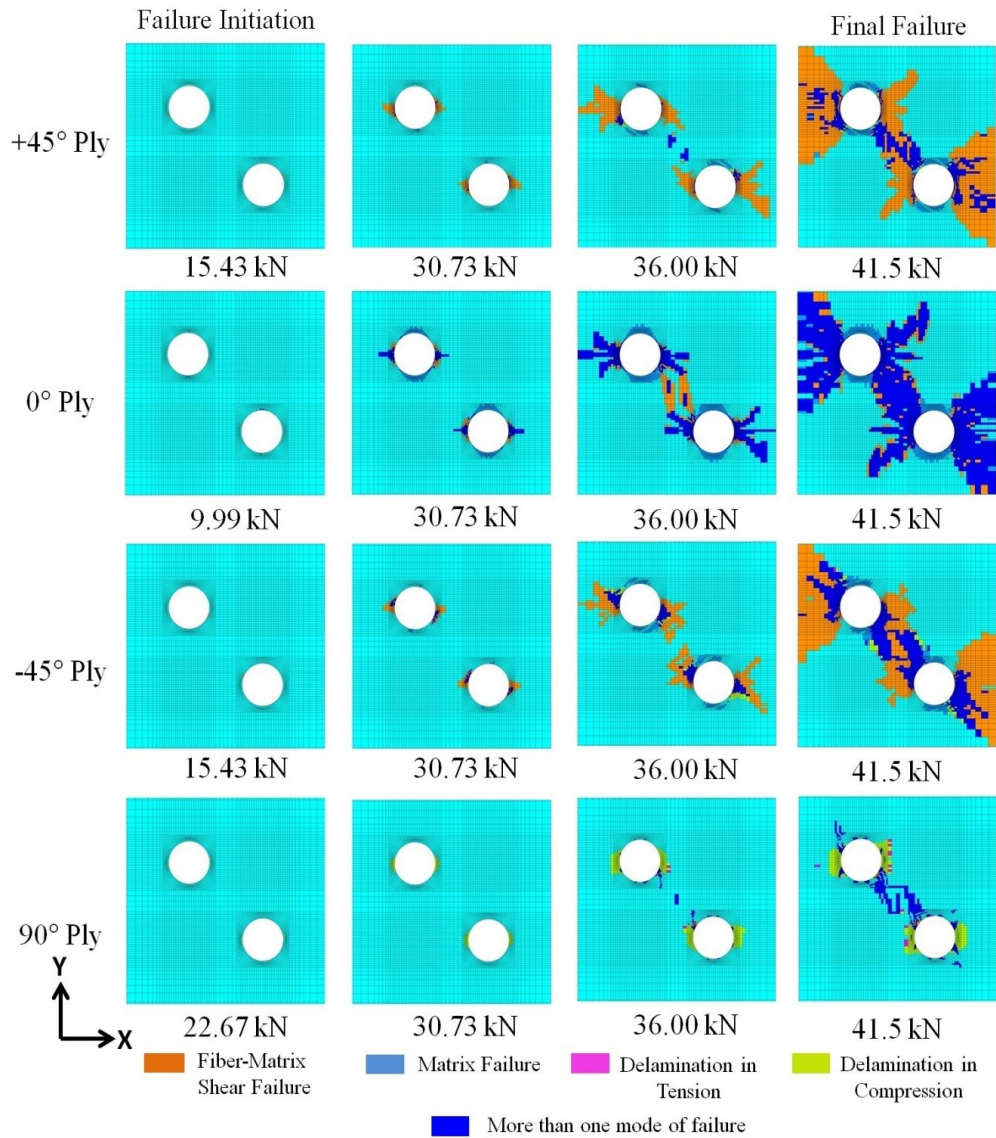
Figure 3.22: Illustration of damage propagation predicted by the PDM with increasing load for $[+45/0/-45/90]_{2S}$ laminate having 2HD configuration.
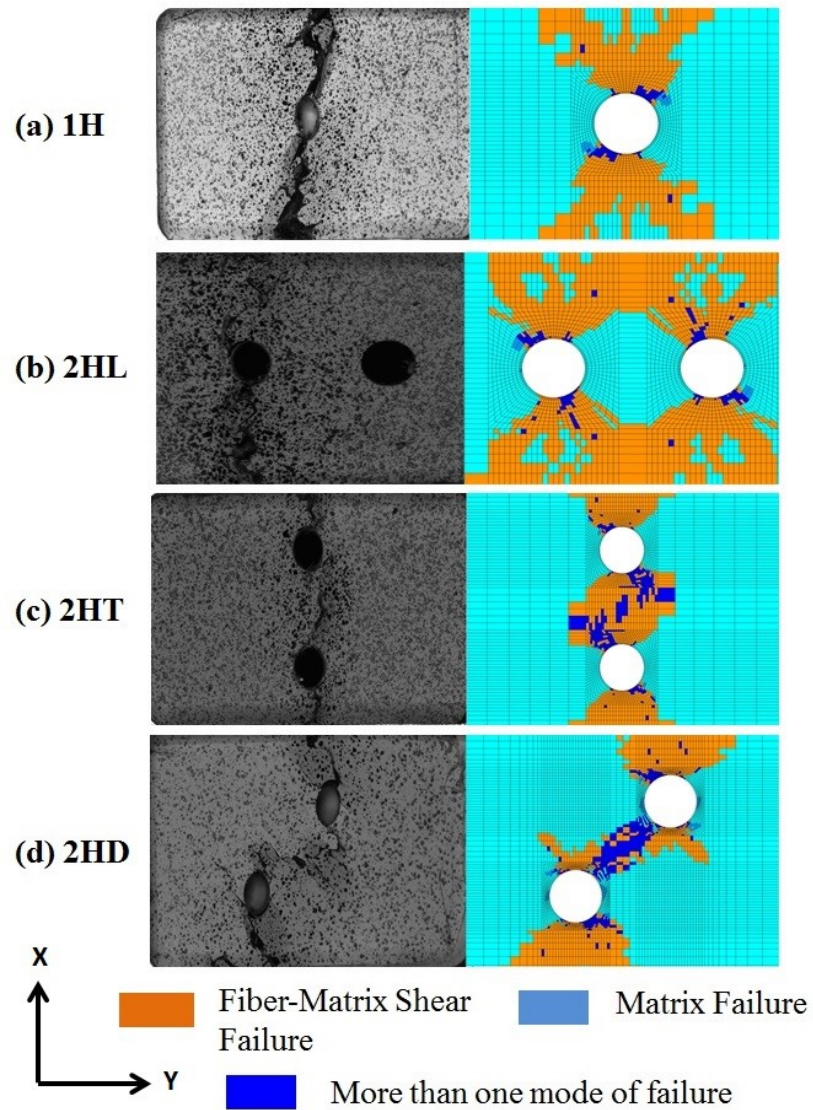
Figure 3.23: Final Failure comparison in panel with different hole configurations of Experimental and PDM prediction

Chapter 4

Progressive Damage Analysis of External Bonded Patch Repair under Compression

4.1 Introduction

In this chapter, a three dimensional finite element based PDM is presented for single-sided and double-sided bonded patch repaired CFRP laminates subjected to compressive loading. The developed model is suitable for predicting failure and post failure behavior of bonded patch repaired in fiber reinforced composite materials. It can also predict the final failure modes near the hole around the patch. The material is assumed to behave as linear elastic until final failure. The stress values are estimated using three dimensional finite element analysis and damage prediction is done using Hashins failure criterion for unidirectional composite laminates as explained in previous chapter. Damage modeling is accomplished using MPDM. Load-deflection behavior as well as path of damage progression is predicted by both PDM simulation and experiment. They are found to be in good agreement thereby confirming the accuracy of PDM implementation. The modes of final failure near patch repair are predicted by PDM which are in coherence with the experimental observation.

4.2 Problem Description

In this study, carbon/epoxy composite laminates having single-sided and double-sided bonded patch repaired configurations are considered. The panel is of $[+45/0/-45/90]_{2S}$ configuration.The specimen geometry and the test methods used in this study to determine the compressive strength of the bonded repair CFRP composite laminates are from the recommendations from ASTM D 6484 [10]. A slight modification to the standard is considered for fabrication of the anti-bucking compression test fixture to view the bonded patch repair.

The length (L), width (W) and the thickness (t) of the panel are 305 mm, 36 mm and 6 mm respectively are obtained from 350 x 350 x 6 mm panels. We choose diameter (D) of the holes of length 5 mm. This choice of the hole diameter enables (W/D ¿3.5) to limit the edge effects. The CFRP specimens of different configurations (1H, SSR, DSR), as shown in the Fig. 4.1 are analyzed in this work. Configuration 1H contains an open cutout at the center, SSR contains single sided bonded repair and DSR contains double sided bonded repair. The rounded-composite patch of parent CFRP having thickness $tp = 3$ mm was bonded using the adhesive material (Araldite 2011), as shown in the Fig. 4.1.
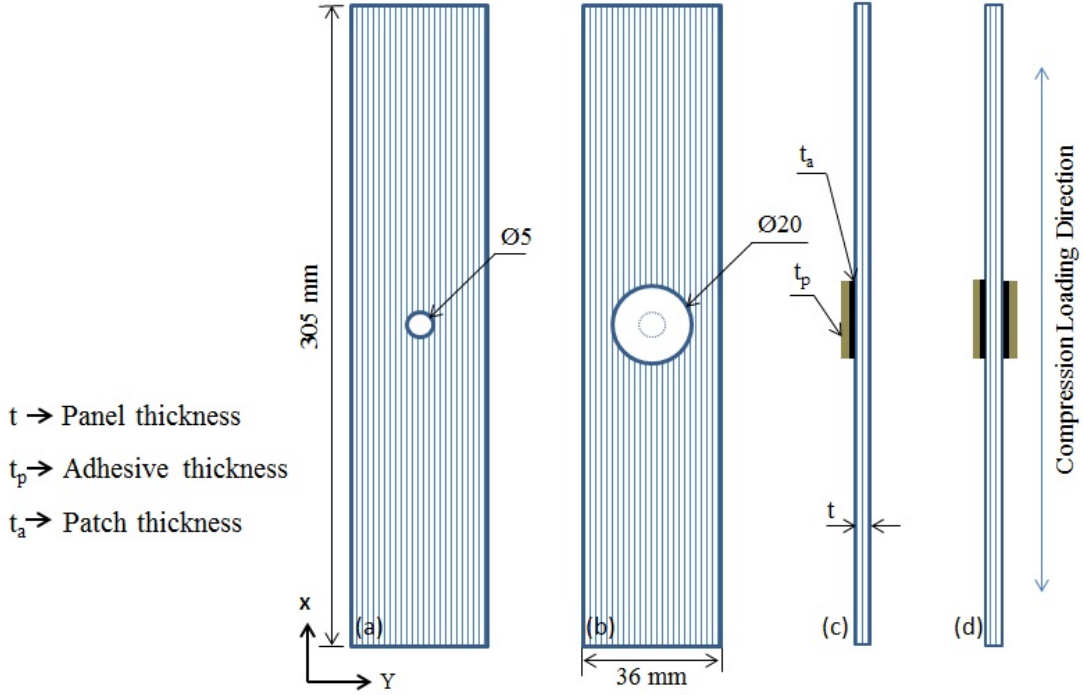
Figure 4.1: Specimen geometry (a) open cutout panel (b) repaired panel (c) single-sided repaired panel (d) double-sided repaired panel (All dimensions are in mm)

4.3 Experimental Study

4.3.1 Specimen Preparation and Experimental Setup

The specimen comprising of the patch and panel are prepared from composite laminates fabricated in-house using hand layup technique. The composite laminates are made of UD carbon fiber mat (supplied by Golbond) of 230 gsm. The matrix is made from epoxy resin LY-556 mixed with hardener HY-951 from Huntsman grade in the ratio of 10:1 by weight. The average thickness of each layer of laminate after casting is of 0.375 mm. Specimens are cut from fabricated laminates using abrasive cutter mounted on the hand-held saw and

then they are machined to the required dimensions with the special diamond-coated end mill (JS520100D3S.0Z6-SIRA) supplied by SECO Jabro Tools. The typical geometry and dimensions of open cutout and repaired specimen is shown in Fig. 4.1. A circular hole of diameter 5 mm is drilled at the center of the panel (see the Fig. 4.1) to simulate the effect of damage removal. This type of removal happens in the case of low velocity impact damage. The cutout panel is then bonded with a circular patch of diameter 20 mm. The patches are bonded using two-part intermediate strength adhesive Araldite 2011 supplied by Huntsman. The adhesive thickness is measured by an optical microscope (Leica DM6000 M) using HCX PL FLUOTAR 5 x/0.15 BD lens at 5X magnification and the average value (ta) of 0.15 mm. The configurations of the quasi-isotropic panel and patch considered in the present study is of stacking sequence $[+45/0/-45/90]_{2S}$ and $[+45/0/-45/90]_{1S}$ respectively. The experimental setup used in the present study is shown in the Fig. 4.2. It consists of a computer controlled MTS Landmark servo-hydraulic machine of 100 kN load capacity. The anti-bucking compression fixture was fabricated at the Central Workshop, IIT Hyderabad as per ASTM D 6484 Standard test method [10]. The dimensions of the anti-bucking compression fixture are such that it prevents buckling failure and ensures only in-plane static compressive load on the specimen. The fixture has been slightly modified with window size of length 40 mm by width 25 mm for viewing the external bonded repair failure. Teflon Tape is placed on the inner walls of the fixture to reduce friction. It increases the flexural stiffness of laminate but does not carry load. The specimen with the anti-buckling fixture is placed between compression platen and aligned properly as shown in the Fig. 4.2. All specimens are loaded in compression and the test is carried out in the displacement control mode at rate 2 mm/min. The load and displacement data values are stored in user interference system from MTS for every 0.006 sec.

The material properties of carbon/epoxy composite laminates used in present study are determined by conducting a series of tests as per ASTM standards. A three dimensional-DIC technique is employed for material characterization and the procedure is outlined in Ref. [13, 57, 58]. The estimated properties are given in Table 4.1.

4.4   Finite Element Modeling

In this section focus is on the development of three dimensional finite element models of an open cutout and its repair using CFRP panel in ANSYS 13. The panel, patch and adhesive is modelled using 20 noded SOLID 186 brick element. The entire model is discretized using a mapped mesh. The region surrounding the hole is fine meshed to capture the high stress gradient around it. A detailed study of mesh design in finite element analysis of composite laminates can be found in the Ref. [59]. A minimum of 96 elements along the circumferential direction is chosen based on the mesh convergence study, as suggested in [60]. In here, the mesh around the circular hole has a total of 147456 elements (that is 96

51
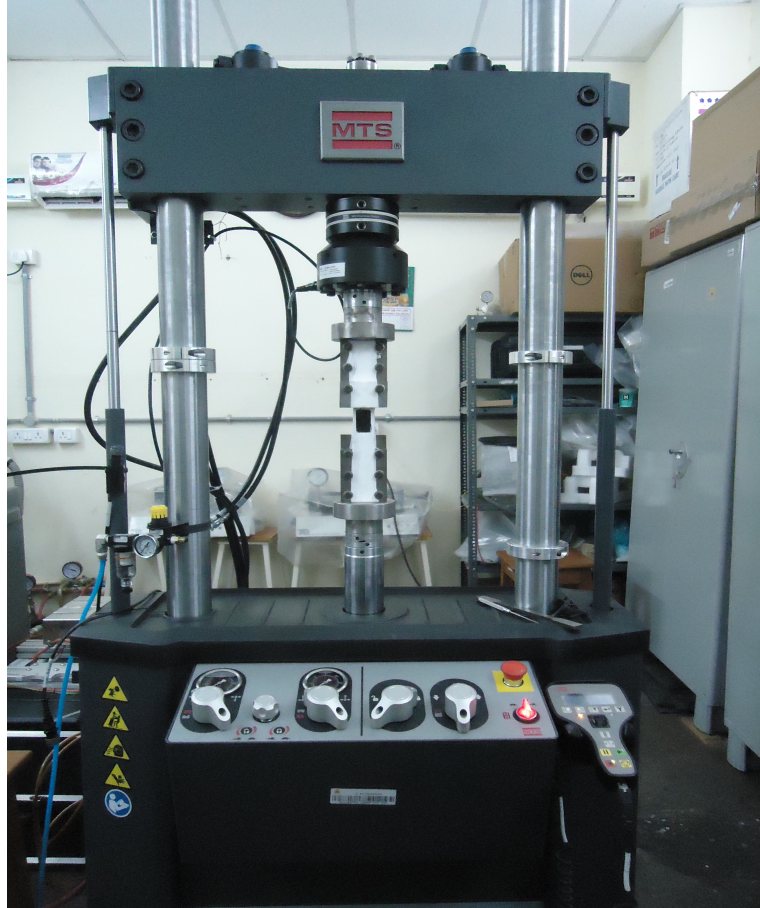
Figure 4.2: Experimental Setup of Compression Anti-buckling fixture with Specimen loaded between Compression Platen

circumferential; 96 radial; 16 elements through the thickness Away from the hole, a coarser mesh has been adopted to reduce the total degrees of freedom so that the computational time can be minimized. Every layer in the panel and patch contains one element in thickness direction. The layer angles are defined by assigning an appropriate element coordinate system. Multi-point constraint (MPC) algorithm is used to ensure perfect bonding between the patch/adhesive and adhesive/panel interfaces. For all the cases, full models are analyzed since symmetry is lost as the damage evolves. The zoomed view of the finite element model of an open cutout and repaired panel is shown in the Fig. 4.3. Material properties obtained from DIC tests are applied to the finite element model (see Table. 4.1). The degree of freedom (dof) along x-direction is constrained on the bottom face of the laminate. The degrees of freedom along y-direction of all the nodes in the top face of the specimen is coupled together and u-displacement is applied at the master node which is located at the center. For better understanding, the schematic representation of the applied boundary condition of the FEA model is shown in the Fig. 4.4

Table 4.1: Material properties of the carbon/epoxy laminate and adhesive [13, 12]

Material properties of the carbon/epoxy laminate	
Longitudinal modulus , E_{xx} (GPa)	84.16
Transverse modulus, $E_{yy} = E_{zz}$ (GPa)	7.12
Shear modulus, $G_{xy} = G_{xz}$ (GPa)	3.30
Shear modulus, G_{yz} (GPa)	2.47
Poisson's ratio (ν_{xy})	0.31
Poisson's ratio (ν_{xz})	0.43
Poisson's ratio (ν_{yz})	0.31
Longitudinal tensile strength, X_T (MPa)	1080
Transverse tensile strength, Y_T (MPa)	35
Longitudinal compressive strength, X_C (MPa)	600
Transverse compressive strength, Y_C (MPa)	90
Shear strength, $S_{xy} = S_{yz}$ (MPa)	57
Shear strength, S_{xz} (MPa)	28.5
Material properties of the Adhesive (Araldite 2011) [57]	
Young modulus , E (GPa)	1.148
Poisson's ratio (ν)	0.40
Shear strength, (MPa)	19.2
Failure shear train	0.047

4.5 Progressive Damage Model

4.5.1 Failure criterion for CFRP laminates

Progressive damage analysis (PDA) is performed based on the assumption that material shows linear elastic behavior until final failure. The process of damage development using PDA is elaborately explained and discussed in the Ref. [48]. There are three major steps involved in Progressive damage modeling (PDM) and they are stress analysis, damage prediction and damage modeling. Stress analysis is done using the commercial finite element package ANSYS 13. Stresses are estimated for each element in the principal material direction of the laminate. Damage prediction in composite laminates is very complicated mainly due to the presence of different failure modes or combination of them. In this study, stress based Hashins failure criterion [52] is employed for predicting the damage initiation as well as damage evolution because of the following reasons. It can predict different modes of failure in a composite structure which is particularly useful for progressive damage modeling because different degradation rules needs to be employed for different modes of failure. Hashins failure criterion is independent of nature of loading and it is widely used by researchers for strength prediction as well as for progressive failure analysis. Since it is a three dimensional failure criterion, Hashins failure criteria can be adopted with three dimensional FEA study. In addition, it can be easily incorporated in ANSYS parametric
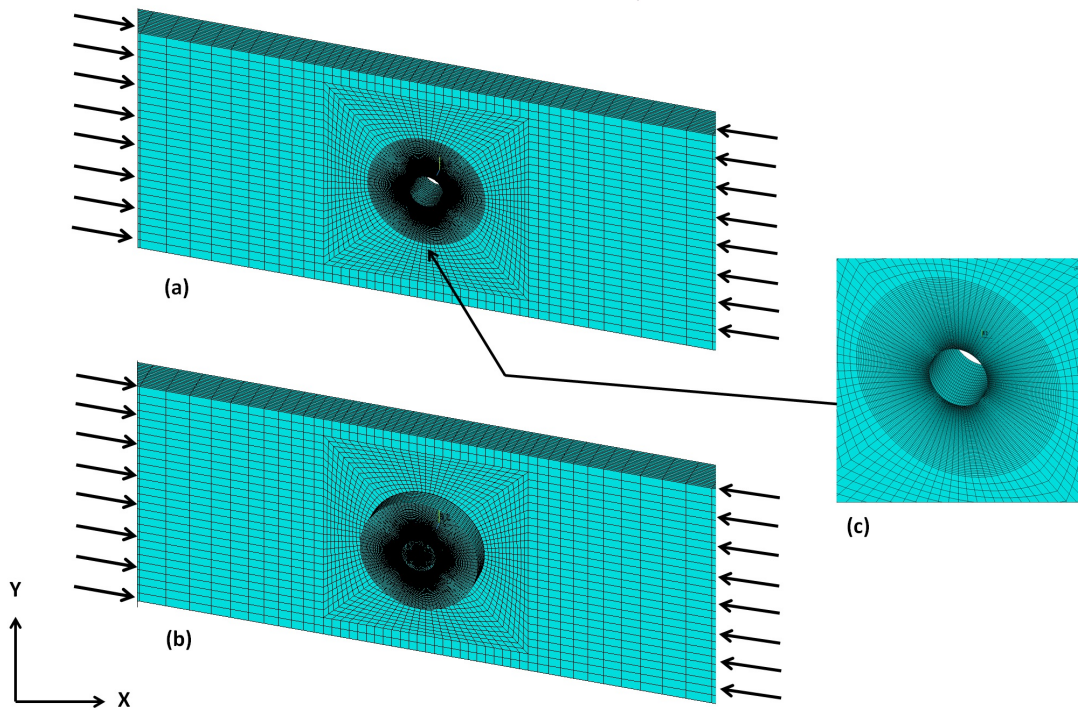
Figure 4.3: Finite element model (a) open cutout panel, (b) repaired panel and (c) (e) Zoomed view of the finite element model around the hole
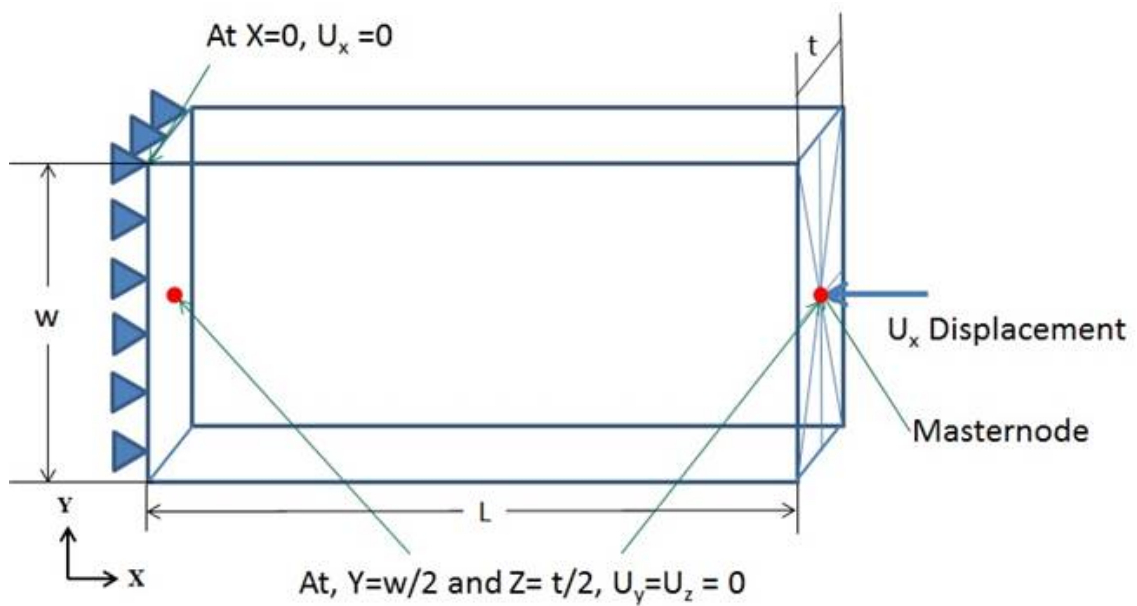

Figure 4.4: Schematic representation of applied boundary condition to FEA model

development language (APDL) code. Eight set criteria are used for predicting eight dif-

ferent modes of failure. These modes of failure include, fiber failure under tensile load, fiber failure under compressive load, matrix failure under tensile load, matrix failure under compressive load, fiber-matrix shear failure in tension, fiber-matrix shear failure in compression, delamination in tension and delamination in compression. The stresses for each element and the material strength values are substituted into Hashins failure criterion for prediction of damage. Once the failure is detected in any of the elements, the damage modeling is done to mimic the loss in the load carrying capacity of the failed element. In the third step, once the damage is detected by a failure theory, a damage modeling technique is then incorporated to take into account the effect of damage on load-bearing capacity of the laminate and further post-damage analysis is performed. This is achieved by degrading the elasticity property of the failed elements and this method is termed as material property degradation method (MPDM) which assumes that the damaged element can be replaced by an equivalent element with degraded material properties. When failure is detected in an element, dominant elastic material properties are degraded to 5% of their actual value according to the degradation rule given in Ref. [48]. The proposed PDM is implemented through ANSYS parametric macro-routine, as depicted in the flowchart shown in the Fig. 4.5. Initially, a three dimensional FE model is developed and analysis is performed by assigning appropriate material properties set to their initial values, boundary conditions, initial displacement value of 0.05 mm and subsequent increment.

4.5.2 Failure criterion for adhesive

In the repaired laminate, the patch debonding is an important failure mode. It is the weakest link in the repaired panel system. The presence of debonding reduces the effective patch area and hence it reduces the load transfer between the patch and panel which in turn affects the load-bearing capacity of repaired laminate. The patch debonding is mainly influenced by the presence of high shear stress/strain in the adhesive layer [19, 42]. The maximum shear stress and strain criterion is used for predicting the failure of adhesive layer at an elemental level as explained in Ref. [43].

4.6 Results and discussions

4.6.1 Results obtained based on PDM simulation

To validate the developed finite element analysis, the longitudinal load-displacement curve predicted by PDM simulation for the unrepaired, single and double-sided bonded repaired panel (Quasi-isotropic) is compared against the corresponding load-displacement obtained from the experiments as shown in Fig. 4.6(a-c) respectively. One can clearly observe that the slope of the load-displacement curve obtained from both PDM and experiment is in close agreement along the longitudinal direction in the composite laminate thereby confirming the accuracy of the implemented PDM algorithm. The choice and implementation
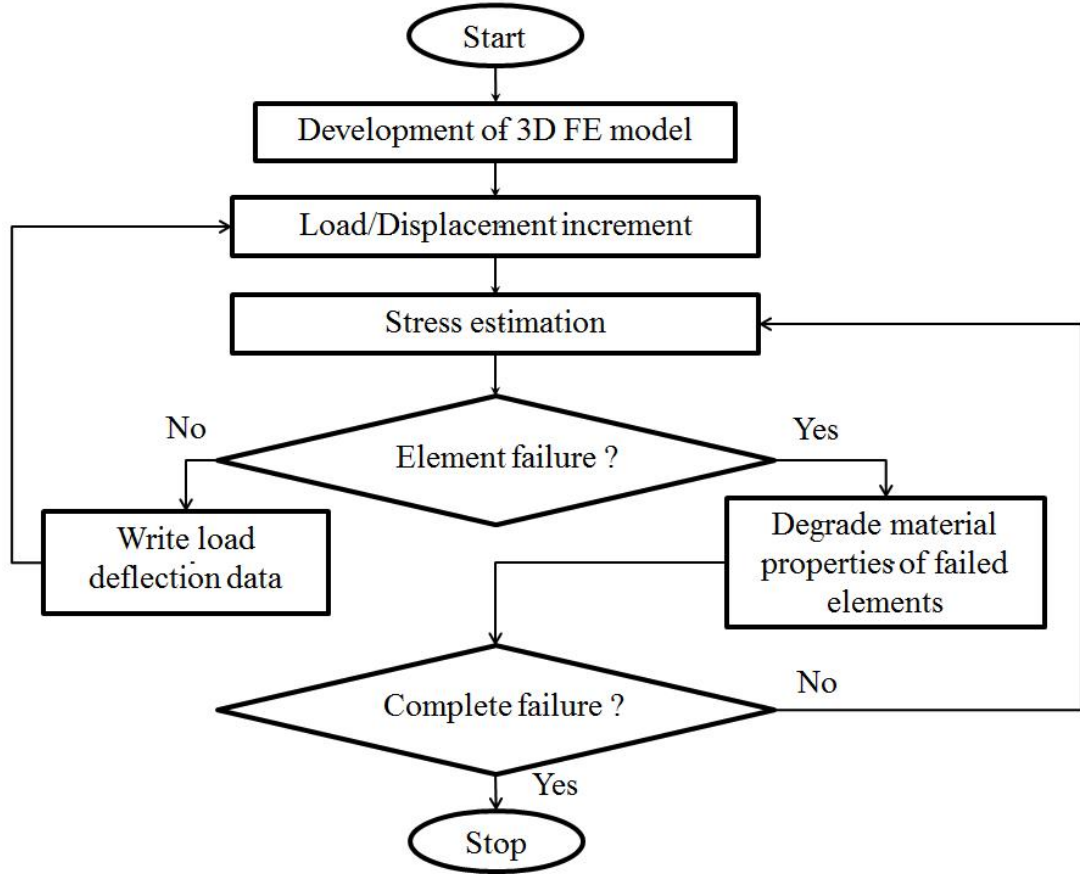
Figure 4.5: Flowchart depicting PDM algorithm

of composite failure theory is very critical in the accuracy of PDM prediction. Besides this, several approximations are involved in the material property degradation rules. The above mentioned factors could be the reason for deviation between PDM and experimental results shown in Fig. 4.6. In Table 4.2 we present failure initiation load (obtained through FEA), at which failure starts (from any mode) in any of the element in the panel predicted by PDM. Further, the ultimate load (load at final failure) predicted from both experiments as well as PDM are also tabulated in Table 4.3. It is observed that composite laminate with double sided repair panel (DSR) sustains highest load before final failure compared to the single sided repair panel (SSR). With the Double sided bonded repair (DSR) techniques, it is clearly observed that the CFRP laminates regain its structural strength by 80 to 85%. In all the configurations it is observed that there is a significant amount of damage accumulation around the hole due to fiber-matrix shear failure, matrix failure and delamination due to both tension and compression. Damage typically initiates from the hole edge and propagates towards the transverse free edge along the net section and eventually patch gets completely debonded from panel.

56

Table 4.2: Failure initiation load and debonding load predicted by PDM

Configuration	Failure Intiation Load (kN)	Debonding Load (kN)
1H	11.65	–
SSR	11.56	18.57
DSR	13.97	20.79
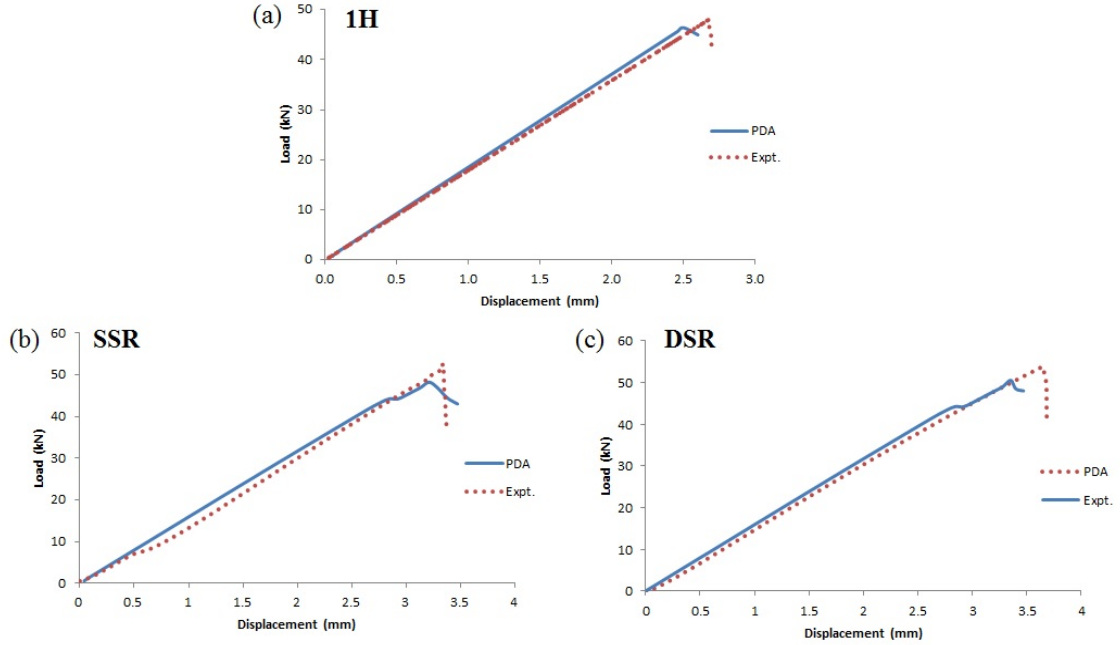
Figure 4.6: Loaddisplacement behavior for panel with different hole configurations (a) Open Cutout (1H) (b) Single Sided Repair (SSR) and (c) Double Sided Repair (DSR)

Table 4.3: Maximum strength and maximum displacement for $[+45/0/-45/90]_{2S}$ panel

Specimen No.	Ultimate Load (kN)		Maximum displacement at failure (mm)	
	Experiment	PDM	Experiment	PDM
1H	47.82±1.23	45.26	2.63±0.17	2.54
SSR	50.63±0.92	48.07	3.25±0.13	3.11
DSR	53.47±1.86	50.52	3.57±0.08	3.35

4.6.2 Open Cut-out CFRP Specimens

Figure 4.7 illustrates the progressive damage in $[+45/0/-45/90]_{2S}$ laminate having open cutout panel (1H configuration) with increasing load. In $0°$ layers, matrix failure and fiber-matrix shearing failure initiate near the hole at a load of 11.85 kN followed by delamination as the damage grows with the load, as shown in Fig. 4.8. Whereas in $45°$ layers, fiber-

matrix shear failure and matrix failure initiate near the hole edge in at a load of 16.42 kN. However, in 90° layers failure initiation is due to delamination in compression along with matrix failure near the hole edge at a load of 22.78 kN followed by delamination in tension as load increases. On further increase in the load, extensive fiber-matrix shear failure occurs in the plies and then delamination failure starts propagating in +45°, 45° and 90° plies across width of the panel, as shown in the Fig. 4.7. Finally, as the load approaches a value of 46.43 kN, the damage propagates very rapidly in normal direction to the loading axis from the transverse hole edge towards the free edge of the laminate, resulting in total failure along the net section. The final damage zone in an open cutout panel predicted by PDM is found to be consistent with the experimental observations, as shown in the Fig. 4.9.

4.6.3   Single-Sided Bonded Repaired CFRP Specimens

The initiation and propagation of damage in the adhesive layer, the patch and in the surface ply (45°) of the panel are shown in Figs 4.11(a-i). In the single-sided repaired panel, fiber-matrix shear failure and matrix cracking are the damage initiation modes seen at load 12.36 kN (See the Fig. 4.10). It is clearly observed that the unsymmetrical repair causes additional bending effects resulting in the neutral axis shift of the repaired panel. Further leads to initiation of the damage on the unpatched surface of the single sided repaired panels. Figures. 4.11(a-i) shows the damage mechanism in the single sided repaired panel predicted by PDM. Similar to the unrepaired panels, the damage initiates in 0° layers around the hole boundary but at a slightly lower load of 11.56 kN. As the load increases, the localized matrix cracking and delamination occur at high stress concentration locations near the patch transverse overlap edge and patch longitudinal overlap edge respectively at a load of 31.23 kN (see Figure 4.11(a)). Further, the damage propagation involves matrix cracking, fiber-matrix shear failure and delamination failure in 0°, +45° and -45° ply transverse to the fiber direction. A partial patch debonding happens due to shear failure in the adhesive layer over the hole edge and from the stress concentration regions at longitudinal overlap edge of the patch (see Figure 4.11(b)). Fewer matrix cracking and delamination are observed at the overlap edge of the patch (see Figure 4.11(c)). As the load increasing, matrix cracking and delamination is get more prominent to start debonding from adhesive. The final failure of the panel takes place soon after complete debonding of the patch at load 48.07 kN. At this juncture, an extensive matrix cracking and fiber-matrix shear failure with the delamination are observed in 45° and 0° plies across the panel width whereas the 90° plies shows a lesser matrix cracking and delamination near hole edges. Once again the damage zone predicted by PDM is found to be in good coherence with the experimental observations, as shown in the Figure 4.11(g)-(l).
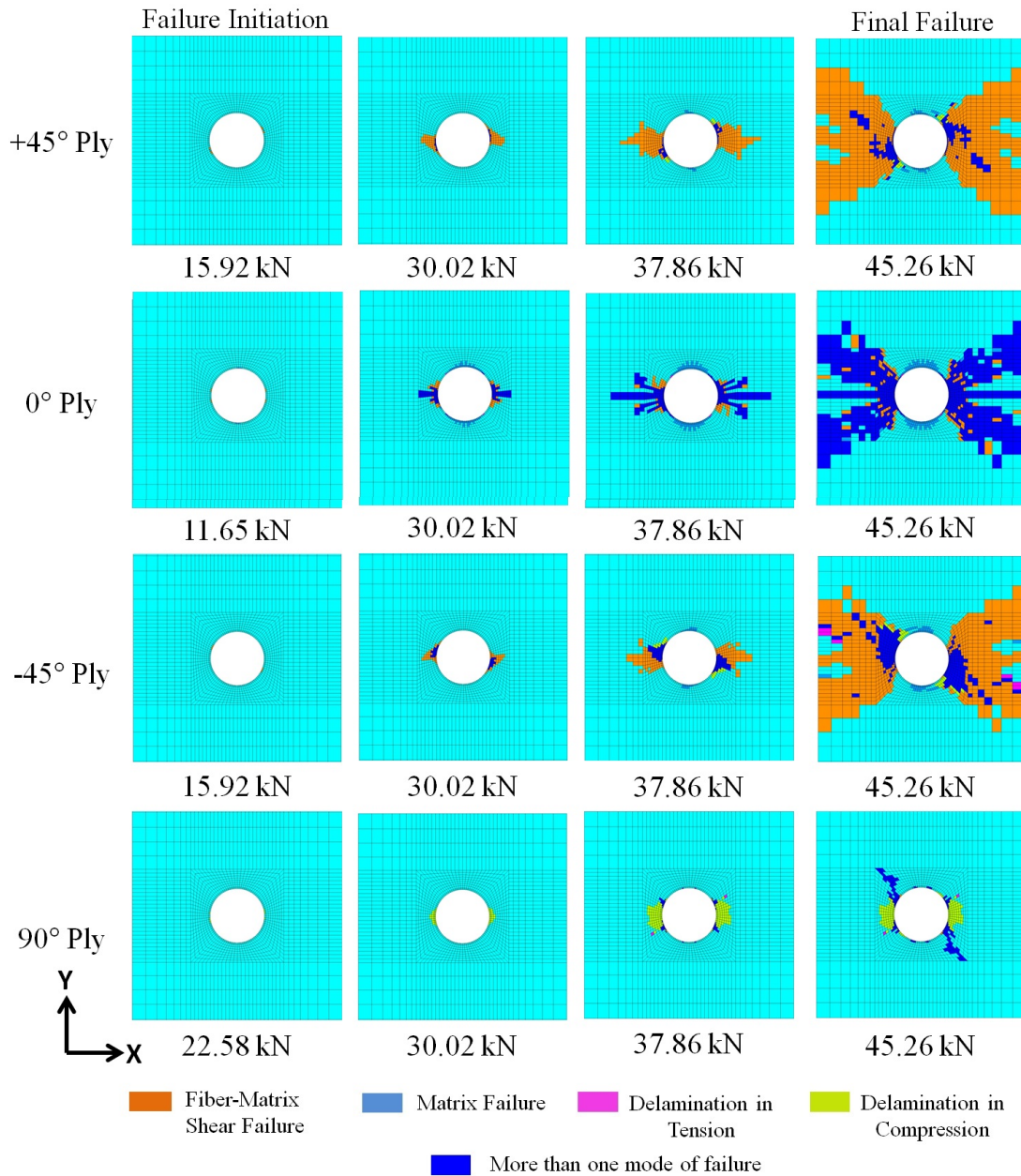
Figure 4.7: Illustration of damage propagation predicted by the PDM with increasing load for $(+45/0/-45/90)_{2S}$ laminate having 1H configuration

4.6.4 Double-Sided Bonded Repaired CFRP Specimens

In case of double-sided repair, the failure initiates with the matrix cracking around the hole edge at a load of 13.97 kN followed by fiber-matrix shear failure as the load increases, as shown in the Fig. 4.12. Figures 4.13(a-i) shows the damage mechanism in the double sided repaired panel predicted by PDM. The failure initiation in the adhesive layer leading to patch debonding is first observed near the longitudinal overlap edge of the patch, as shown
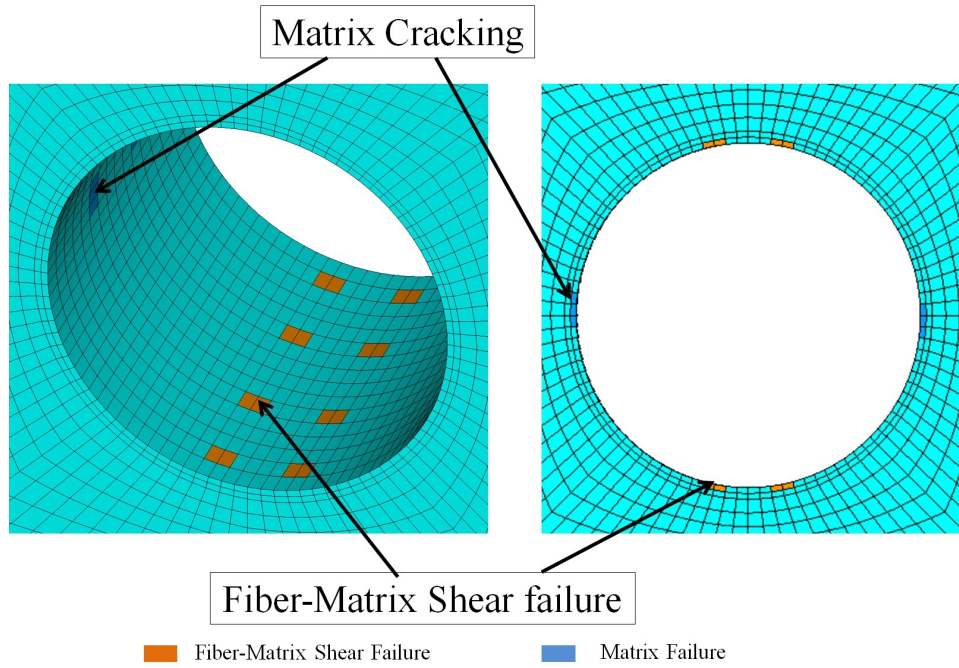
Figure 4.8: Damage initiation site in the 0° layer around the hole in an open cutout quasi-isotropic panel $(+45/0/-45/90)_{2S}$ during compression loading
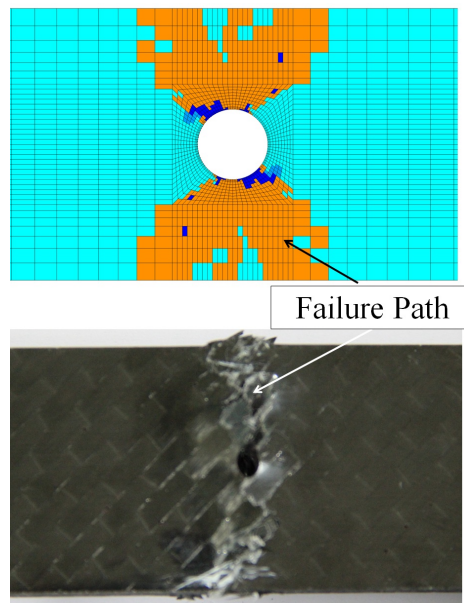
Figure 4.9: Final Failure comparison open cutout panel with Experimental and PDM prediction

in the Fig. 4.13(b) and later around the hole periphery at higher loads. With further increase in the load, the damage propagates in the panel with extensive matrix cracking
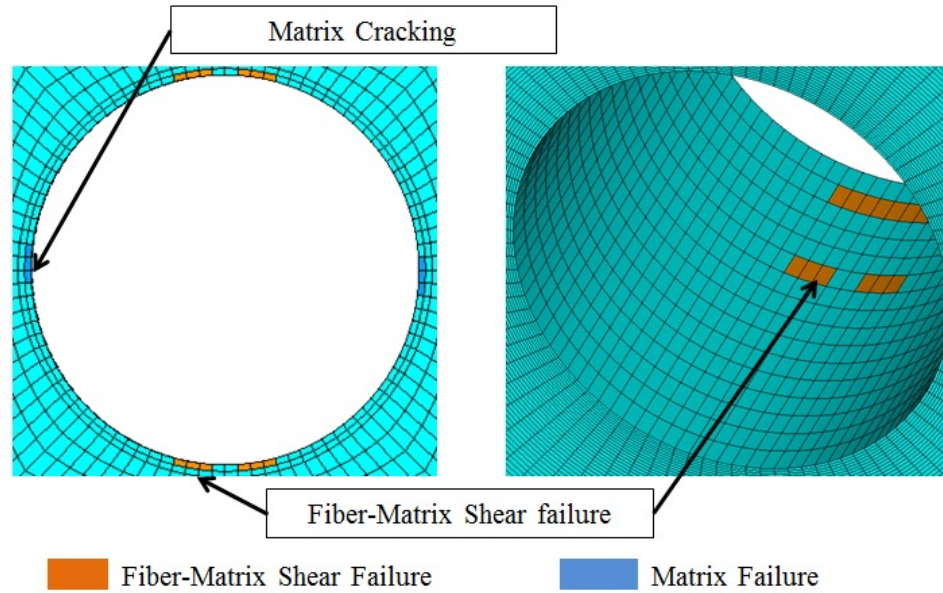
Figure 4.10: Damage initiation site in the 0° 11th layer around the hole in an single sided repair (SSR) quasi-isotropic panel $(+45/0/-45/90)_{2S}$ during compression loading

across the panel width and fiber failure starts propagating in 45° ply (see Fig. 4.13(d)). The final failure of the panel takes place after the complete debonding of the patch at load 50.26 kN. Similar observations are made from the experiment and final failure zone predicted by PDM is found similar to that of experimental behavior as shown in Fig. 4.13(g)(l).

The ultimate strength and maximum displacement value predicted by PDM for all the three quasi-isotropic panels are shown in Table 4.3. Here, the experimental values are compared with the PDM prediction and they are in good agreement. However, the displacement is under-predicted by simulation as explained earlier. Also one can note from the table that the double-sided repair specimen has got higher strength because of more reinforcement as well as in-plane behavior compared to single-sided repair. However, in most of the practical applications the single-sided repair is only possible due to no access to other side.

4.7 Closure

In this work, the progressive damage analysis of both unrepaired and repaired by CFRP panel either single-sided or double-sided CFRP patch is studied using experiments and numerical analysis. The key points of the current study are listed as follows:

- Finite element based 3D PDM is developed for predicting the failure and post failure behavior of quasi-isotropic panels with open cutout under in-plane compression load for 1H, SSR and DSR configurations.

Figure 4.11: Damage mechanism in single-sided repaired quasi-isotropic panel [+45/0/-45/90]$_{2S}$ (a-c) Failure initiation, (d-f) Intermediate failure mechanism and (g-i) Final failure damage path predicted by PDM and (j-l) experimentally observed

- Experiments investigations are carried for 1H, SSR and DSR configuration to obtain the mechanical behavior under pure in-plane compressive load using ant-buckling fixture.

- Stress-based 3D Hashins failure and maximum shear stress and strain based criterion
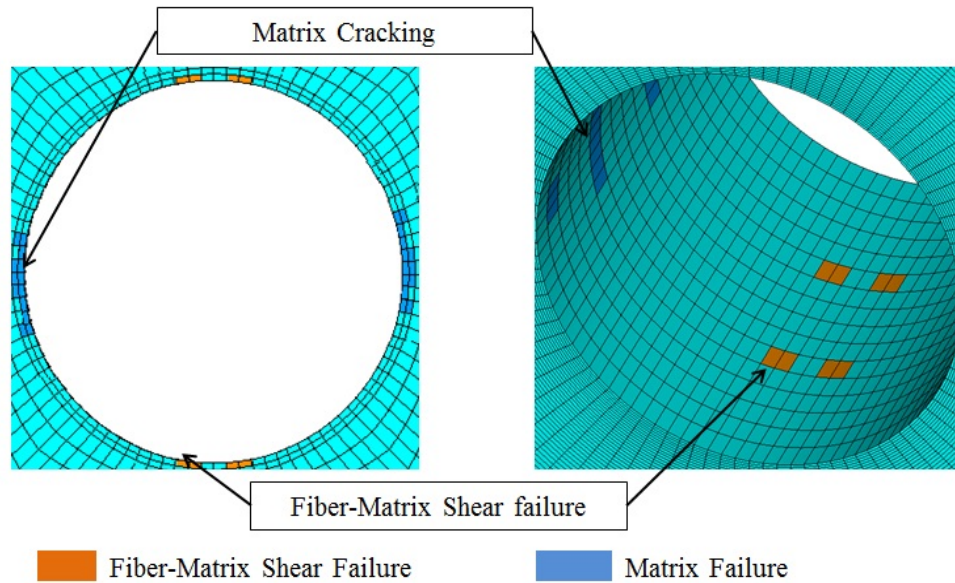
Figure 4.12: Damage initiation site in the 0° 6th layer around the hole in an Double sided repair (DSR) quasi-isotropic panel $(+45/0/-45/90)_{2S}$ during compression loading

are used for predicting the damage in CFRP panels and the adhesive layer respectively.

- Material property degradation method (MPDM) is used to model the damage.

- Damage initiation in quasi-isotropic panels is always observed in 0° layer for all the configurations (1H, SSR, DSR). The damage consists of extensive matrix cracking and fiber-matrix shear failures running along it in $\pm 45°$ and 0∘ plies across the width of the panel.

- Final failure in repaired panels is observed only after the complete debonding of patch has taken place due to shear failure in the adhesive layer.

- The patch debonding behavior of single-sided repaired panel is quite different from double-sided repaired panel configuration. In case of the single-sided repaired panel, the patch debonding initiates from the patch overlap edge and around the hole edge whereas, it initiates only from the patch overlap edge in the double-sided repaired panel.

- Failure initiation load of single-sided repair configuration 0.8% less than the unrepaired configuration. However, the final failure load of single-sided repair configuration is 5.9% higher than unrepaired configuration.

- The ultimate strength and damage progression predicted by PDM are found to be consistent with the experimental observations thereby confirming the accuracy of the developed PDM in conjunction with finite element method.
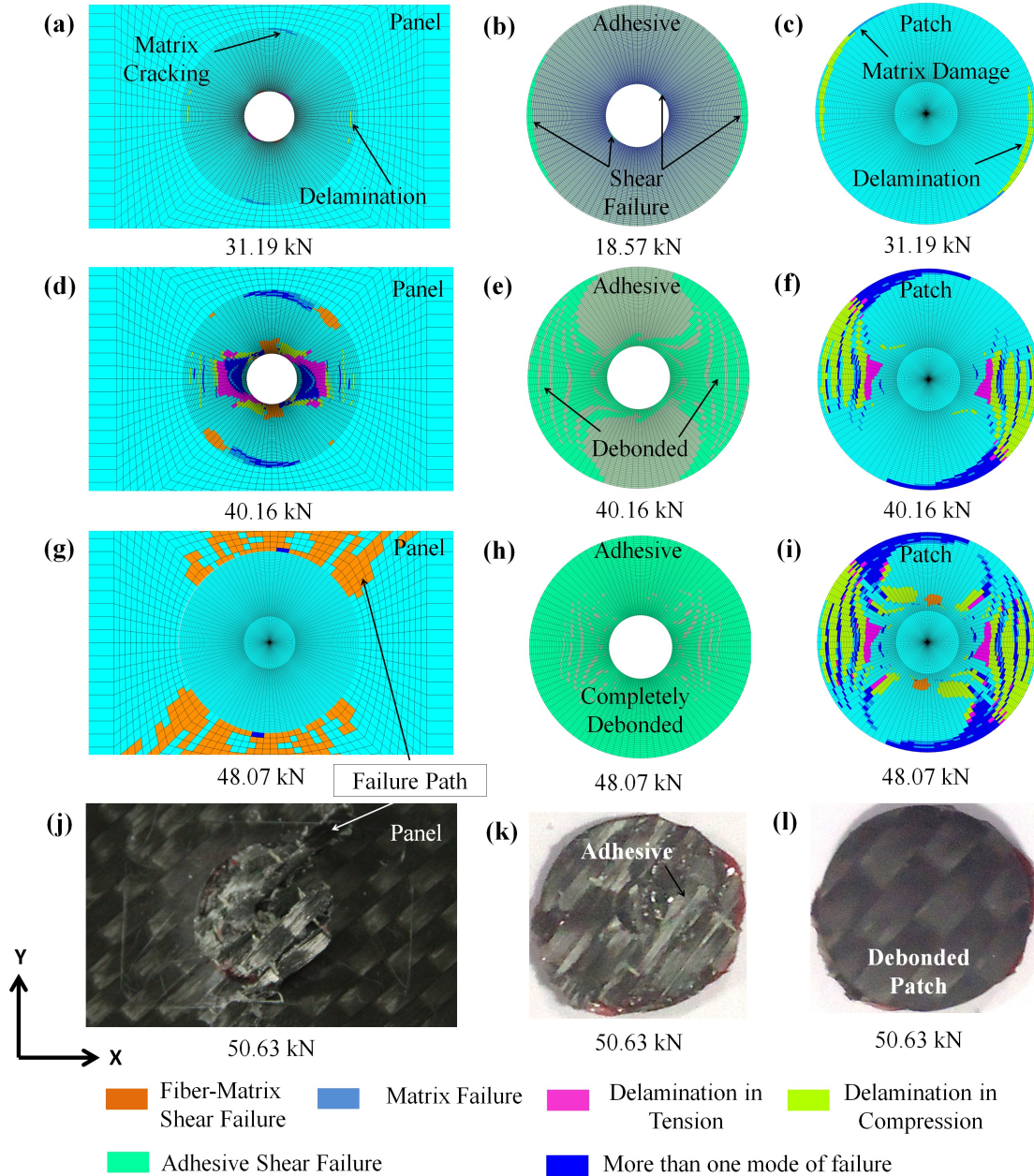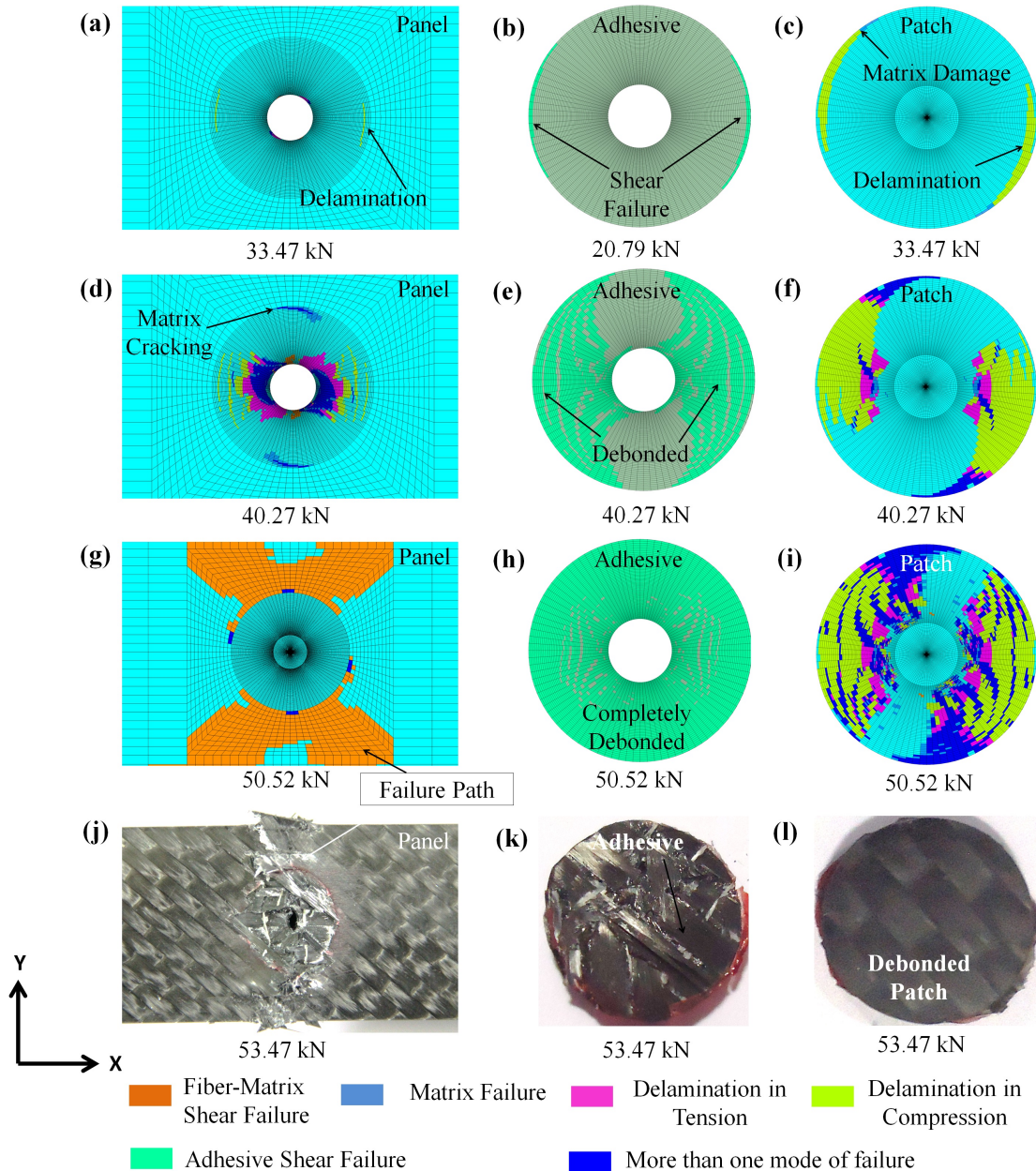
Figure 4.13: Damage mechanism in double-sided repaired quasi-isotropic panel $[+45/0/-45/90]_{2S}$ (a-c) Failure initiation, (d-f) Intermediate failure mechanism and (g-i) Final failure damage path predicted by PDM and (j-l) experimentally observed

- Kushfuddoja et. al. [48] obtained the whole field displacements and strain components using DIC in their study of repaired CFRP panel subjected to tensile loading. However, we could not reproduce the same under compressive loading due to experimental limitations. That is in order to perform DIC, a bigger window is require to

carry out the image capturing, but in order to avoid buckling during compression it is not feasible to provide bigger window in anti-buckling fixture which limited us to obtain the whole field displacements and strains.

Double-sided repaired configurations sustained maximum load. And it has got higher initiation and final failure load among all other configurations. Further, in the DSR configuration there is 85% restoration of the strength compared to the virgin sample (see Table. 4.3). Hence we recommend the double-sided patch repair over the single-sided patch for the CFRP panels loaded under compression.

Chapter 5

Conclusion and Recommendations for Future Work

In this work, first discussed about the various compression test method and studied the comparision between SACMA and UCSB test method. UCSB test method would be good alternate option for compression test as it is light weight, require smaller specimen and provide consistent and accurate results.

Followed by a three dimensional finite element based progressive damage model is developed for fiber reinforced composite laminates and it is applied to CFRP laminates having multiple holes and also to bonded repaired in CFRP laminates. The developed model is suitable for predicting failure and post failure behavior of the laminates. The three basic steps involved in PDM are stress analysis, failure analysis and damage propagation. Whole field surface strain analysis of the composite laminates is performed using digital image correlation experiments. Finite element model is first validated by comparing whole field surface strains and displacements obtained from FEA with those from DIC experiment. Load deflection behavior predicted by PDM is also compared with the experimental behavior and is found to be in good agreement. Path of damage progression predicted by PDM is in line with the experimental observations there by confirming the accuracy of the PDM algorithm developed. For the mulitple hole and bonded repaired configurations in CFRP laminates, the final failure modes predicted by PDM are in coherence with experimental observations.

The study can be extended to investigate the damage progression for interacting hole and bonded repair panel under compression using infrared technique (NDT) can be explored to detect and ensure the proper bonding at the interface between patch and panel.

Compressive behaviour of composite material need to study in micro-mechanic based multi-scale modelling. Multi-scale modelling will give ply-wise accurate prediction and will help in comparing the developed PDM.

The present study progressive damage analysis can be extended to compare the predic-

tive capability of different interactive and non-interactive failure theories such as Tsai Wu, Puck Failure, Tsai-Hill, Hoffman, etc. towards bonded patch repair application. Their prediction could be compared with the each other and experimental results for their accuracy.

References

[1] http://arch5541.wordpress.com/2013/01/08/the-great-metal-tube-in-the-sky.

[2] http://www.compositesworld.com/articles/in-situ-composite-repair-builds-on-basics.

[3] D. H. Woolstencroft, A. R. Curtis, and R. Haresceugh. A Comparision of Test Techniques Used for the Evaluation of the Unidirectional Compressive Strength of Carbon Fibre-Reinforced Plastic. *Composites* 12, (1981) 275–280.

[4] Standard Test Method for Compressive Properties of Polymer Matrix Composite Materials with Unsupported Gage Section by Shear Loading 1988. ASTM D 3410.

[5] D. F. Adams. Current Status of Compression Testing of Composite Material. Anaheim, Calif, May 1995 367–371.

[6] Open Hole Compression Test Method, Northrop Corporation, Hawthorne, California 1988. Northrop Specification NAI-1504C.

[7] J. Bardis, K. Kedward, J. Bish, and T. Tsotsis. Alternate compression test method for notched and unnotched composites. volume 45. 2000 .

[8] P. Diwan and N. Fox. Carbon Fibre Technology. Deep & Deep Publications, 1992.

[9] Standard Test Method for Compressive Properties of Rigid Plastics 1985. ASTM D695.

[10] Standard test method for open-hole compressive strength of polymer matrix composite laminates 1999. ASTM D 6484M.

[11] Ubaid J, Kashfuddoja M, and Ramji M. Strength prediction and progressive failure analysis of carbon fiber reinforced polymer laminate with multiple interacting holes involving three dimensional finite element analysis and digital image correlation. *International Journal of Damage Mechanics* 1–27. DOI: 10.1177/1056789513504123 .

[12] Kashfuddoja M and Ramji M. Whole-field strain analysis and damage assessment of adhesively bonded patch repair of CFRP laminates using 3D-DIC and FEA. *Composites: part B* 53, (2013) 46–61.

[13] Mallick P. Fiber reinforced composites: materials, manufacturing, and design. 3rd edition. CRC Press, New York, 2007.

[14] R. Jones. Mechanics Of Composite Materials. Materials Science and Engineering Series. Taylor & Francis, 1998.

[15] Composites Market Report 2013: Market developments, trends, challenges and opportunities Sept. 2013. AVK (Federation of Reinforced Plastics).

[16] Fleck NA and Budiansky B. Compressive failure of fiber composites. *Journal of the Mechanics and Physics of Solids* 41, (1993) 183–211.

[17] Hallett SR and Wisnom MR. Experimental investigation of progressive damage and the effect of layup in notched tensile tests. *Journal of Composite Materials* 40, (2006) 119–141.

[18] A. C. Okafor, N. Singh, U. Enemuoh, and S. Rao. Design, analysis and performance of adhesively bonded composite patch repair of cracked aluminum aircraft panels. *Composite Structures* 71, (2005) 258 – 270.

[19] C. Soutis and F. Z. Hu. Design and performance of bonded patch repairs of composite structures. *Proceedings of the Institution of Mechanical Engineers, Part G: Journal of Aerospace Engineering* 211, (1997) 263–271.

[20] Rosen BW. Mechanics of composite strengthening. *Fiber Composite Materials, American Society for Metals* 37–75.

[21] Guynn EG and Bradley WL. Measurements of the stress supported by the crush zone in open composite laminates loaded in compression. *Journal of Reinforced Plastics and Composites* 8, (1989) 133–149.

[22] Guynn EG, Bradley WL, and Elber W. Micromechanics of compression failure in open hole composite laminates. *Composite Materials: Fatigue and Fracture* 2, (1989) 118–136.

[23] Barenblatt GI. The Mathematical theory of equilibrium cracks in brittle fracture. *Advance in applied mechanics* 7, (1960) 55–129.

[24] Soutis C and Fleck NA. Static Compression Failure of Carbon Fiber T800/924c Composite Plate with a Single Hole. *Journal of composite Material* 24, (1990) 536–558.

[25] Soutis C, Curtis PT, and Fleck NA. Compressive failure of notched carbon fiber composites. In Proceeding of the Royal Society of London, volume 440 of *A*. 1993 241–256.

[26] Soutis C. Measurement of the static compressive strength of carbon-fiber/epoxy laminates. *Composite Science and Technology* 42, (1991) 373–392.

[27] Bazzant ZP, Kim J-J H, Daniel IM, Becq-Giraudon E, and Zi G. Size effect on compression strength of fiber composite failing by kink band propagation. *International journal of Fracture* 95, (1999) 103–141.

[28] M. Abdallah and R. Westberg. An Experimental and Analytical Evaluation of Three Compressive Test Methods for Unidirectional Graphite/Epoxy Composites. *Report No. MISC-E524-10, Hercules Inc* Magna, UT.

[29] C. Gedney, C. Pascual, F. Kolkailah, and B. Wilson. Comparison of ASTM Standard Compression Test Methods of Graphite/Epoxy Composite Specimens. April 1987 1015–1024.

[30] H. J. G. and M. F. L. The Influence of Test Method on The Compressive Strength of Several Fiber Reinforced Plastics. *Journal of Advanced Materials* 25, (1993) 35–45.

[31] J. Berg and D. Adams. An Evaluation of Composite Material Compression Test Methods. University of Wyoming, Laramie, WY, June 1988 .

[32] A. Pearson. Capabilities of Compression Test Methods for Evaluating Unidirectional Carbon Fiber Reinforced Composites. University of Wyoming, Laramie, WY, June 1988 .

[33] Carl R Schultheisz and Anothony M Waas. Compressive failure of composites, Part 1: Testing and micromechanical theories. *Progress in Aerospace Sciences* 32, (1998) 1–42.

[34] A. Hodge, A. Nettles, and J. J.R. Status and summary of test method standardization of advanced composites in japan. 2011 .

[35] Soutis C, Fleck NA, and Smith PA. Failure prediction technique for compression loaded carbon fiber epoxy laminate with open holes. *Journal of Composite Materials* 25, (1991) 1476–1497.

[36] Soutis C, Smith FC, and Matthews FL. Predicting the compressive engineering performance of carbon fiber-reinforced plastics. *Composites Part A: Applied Science and Manufacturing* 31, (2000) 531–536.

[37] Chang FK and Chang KY. A Progressive damage model for laminated composites containing stress concentrations. *Journal of Composite Materials* 21, (1987) 834–855.

[38] Tay TE, Liu G, Tan VBC, Sun XS, and Pham DC. Progressive Failure Analysis of Composites. *Journal of Composite Materials* 42, (2008) 1921–1966.

[39] Wang, D. Y. and Wen, W. D. Three-dimensional progressive damage analysis of composite laminates containing a central hole subjected to compressive loading. In International Conference on Mechanical Engineering and Material Science. 2012 367–371.

[40] Ridha M and Tay TE. Progressive damage analysis of open-hole composite plate under compression. In 18th International conference on composite materials. 2012 .

[41] C. Soutis, D.-M. Duan, and P. Goutas. Compressive behaviour of CFRP laminates repaired with adhesively bonded external patches. *Composite Structures* 45, (1999) 289 – 301.

[42] F. Hu and C. Soutis. Strength prediction of patch-repaired CFRP laminates loaded in compression. *Composites Science and Technology* 60, (2000) 1103 – 1114.

[43] X. Liu and G. Wang. Progressive failure analysis of bonded composite repairs. *Composite Structures* 81, (2007) 331 – 340.

[44] Ridha M and Tay TE. Progressive failure of notched and repaired composite. In 17th international conference on composite materials (ICCM-17). Edinburgh, UK, 2009 .

[45] M. Ridha, V. Tan, and T. Tay. Traction-separation laws for progressive failure of bonded scarf repair of composite panel. *Composite Structures* 93, (2011) 1239 – 1245.

[46] P. Cheng, X.-J. Gong, D. Hearn, and S. Aivazzadeh. Tensile behaviour of patch-repaired CFRP laminates. *Composite Structures* 93, (2011) 582 – 589.

[47] V. S. Bhise, M. Kashfuddoja, and M. Ramji. Optimization of circular composite patch reinforcement on damaged carbon fiber reinforced polymer laminate involving both mechanics-based and genetic algorithm in conjunction with 3D finite element analysis. *Journal of Composite Materials* .

[48] Kashfuddoja M and Ramji M. An experimental and numerical investigation of progressive damage analysis in bonded patch repaired CFRP laminates. *Journal of Composite Materials* 1–18. DOI : 10.1177/0021998314521058.

[49] Sivashanker, S. Damage growth in carbon fibre-PEEK unidirectional composites under compression. *Material Science and Engg. A* 249, (1998) 259–276.

[50] J. Camposneschi. Compression of Compsite Material: A Review. Technical Report pp. 1-55, David Taylor Research Center Nov. 1987.

[51] T. A. Bogetti, J. W. G. Jr, and R. B. Pipes. Evaluation of the IITRI compression test method for stiffness and strength determination. *Composites Science and Technology* 32, (1988) 57 – 76.

[52] Hashin Z. Failure criteria for unidirectional fiber composites. *Journal of Applied Mechanics* 47, (1980) 329–334.

[53] Camanho PP and Mathews FL. A progressive damage model for mechanically fastened joints in composite laminates. *Journal of Composite Materials* 33, (1999) 2248–2280.

[54] Kermanidis D, Labeas G, and Tserpes KI. Finite element modeling of damage accumulation in bolted composite joints under incremental tensile loading. In European congress on computational methods in applied sciences and engineering. 2000 .

[55] McCarthy CT, McCarthy MA, and Lawlor VP. Progressive damage analysis of multi-bolt composite joints with variable bolt-hole clearances. *Composites Part B: Engineering* 36, (2005) 290–305.

[56] Sanchez CM and Greene MJ. Evaluation of Progressive Failure Analysis and Modeling of Impact Damage in Composite Pressure Vessels. *Internship Report, NASA USRP, 2011* .

[57] Araldite 2011. Structural Adhesive, Technical Data Sheet, Huntsman, (2009).

[58] M. Kashfuddoja, R. Prasath, and M. Ramji. Study on experimental characterization of carbon fiber reinforced polymer panel using digital image correlation: A sensitivity analysis. *Optics and Lasers in Engineering* 62, (2014) 17 – 30.

[59] T. Tay, F. Shen, K. Lee, A. Scaglione, and M. D. Sciuva. Mesh design in finite element analysis of post-buckled delamination in composite laminates. *Composite Structures* 47, (1999) 603 – 611. Tenth International Conference on Composite Structures.

[60] Kashfuddoja M and Ramji M. 3-D progressive failure analysis of bonded patch repaired CFRP laminates under tensile load. In Asian conference on mechanics of functional materials and structures (ACMFMS). IIT Delhi, India, 58 December, 2012 .